

Electron momentum spectroscopy of atoms, molecules, and thin films

V G Neudatchin, Yu V Popov, Yu F Smirnov

Contents

1. Introduction	1017
2. Theory of quasi-elastic knock-out of electrons at high energies	1020
2.1 General formalism; 2.2 Electron orbitals in molecules; 2.3 Electron wave functions in a solid	
3. Electron momentum spectroscopy of atoms	1023
3.1 Atoms as a bridge to quantum chemistry; 3.2 Helium as the simplest target;	
3.3 Corrections to a plane wave impulse approximation	
4. Electron orbitals in molecules	1029
5. Electron orbitals in crystalline and amorphous solids	1033
6. (e, 3e) ionization and electron – electron correlation spectroscopy	1038
6.1 Choice of kinematics; 6.2 Large transferred momenta. General formalism; 6.3 (e, 3e) spectroscopy of electron correlations; 6.4 Comparative analysis of (e, 3e) and (γ , 2e) techniques for studying electron correlations	
7. Conclusions	1042
References	1042

Abstract. A review of the theory of electron momentum spectroscopy (EMS) based on the single (multiple) electron impact ionization of a quantum target (atom, molecule, thin film) is presented. Numerous examples are considered which demonstrate the advantages of EMS for interpreting the momentum distributions of the ejected electrons compared to other methods used for direct studies of the many-body wave function of a target. In particular, it is shown that EMS provides considerable progress in the quantum chemistry of molecules and gives a better understanding of processes leading to rearrangement of their outer electron orbitals upon their adiabatic approach. In addition, EMS allows one to study in detail the band structure and form of one-electron wave functions for both crystalline and amorphous thin films. The possibility of direct ‘portraying’ of electron correlations in atoms using the double ionization technique is also considered.

1. Introduction

Experimental determination of the electron wave functions in atoms, molecules, and solids have long attracted the attention of researchers. Historically, a steady tendency is observed of passing from the methods providing a global, general picture to more detailed microscopic information. For example, the

electron diffraction technique successfully employed in this field [1] deals with the angular distributions of elastically scattered high-energy electrons. This allows one to determine with good accuracy the general pattern of the electron cloud and the spatial distribution of the total electron density.

The one-particle wave functions $\psi_i(\mathbf{q})$ in the momentum representation are being extensively studied. Thus, the total momentum distribution (MD) of electrons $\sum_i |\psi_i(\mathbf{q})|^2$ is measured in the reaction $e^+e^- \rightarrow 2\gamma$ of annihilation of a positron with one of the electrons of the system (positrons annihilate in matter after slowing down to the thermal energy) [2]. In experiments, the angular correlation of two photons with energies of about 500 keV is studied in the range of θ in the vicinity of 180° (i.e. the dependence of the coincidence rate on the angle θ between photons). The observed small deviation of the angle θ from 180° is explained by the fact that at ‘some point’ during annihilation an electron interacting with a positron has the momentum \mathbf{q} with a nonzero component perpendicular to the line of photons bouncing apart. The angular correlation curve is used for reconstruction of the electron transverse MD, which includes contributions from a quite broad group of orbitals i , because the energy resolution ΔE for 500-keV photons is rather poor.

The technique of (γ , e) photoelectron spectroscopy (PES) permits the study of individual electron orbitals i [3, 4]; however, this mainly concerns measurements of the binding energy of electrons. In experiments with solids, the angular distributions of photoelectrons relative to the direction of a photon beam are usually measured, and the valent states are analyzed with the help of photons with energy $E_\gamma = 50–60$ eV, which eliminates uncontrollable losses of the emitted electrons and provides high energy resolution $\Delta E \approx 0.02$ eV [5]. The PES technique is called ARPES (angle-resolved photoelectron spectroscopy) in the foreign literature. Because the momentum of the ejected electron is two orders of magnitude greater than that of the photon, the latter transfers its energy to the bound electron, almost not

V G Neudatchin, Yu V Popov, Yu F Smirnov
Scientific Research Institute of Nuclear Physics,
M V Lomonosov Moscow State University
119899 Moscow, Vorob'evy Gory, Russian Federation
Tel.: (7-095) 939-4905; 939-5047
Fax: (7-095) 939-0896
E-mail: popov@srldan.npi.msu.su

Received 23 October 1998; revised 1 August 1999
Uspekhi Fizicheskikh Nauk 169 (10) 1111–1139 (1999)
Translated by M N Sapozhnikov; edited by A Radzig

changing its virtual momentum \mathbf{q} (an analog of the ‘vertical transition’ in optics). As a result, the kinetic energy of the ejected electron is $E_\gamma + \varepsilon_i \simeq q^2/2m$. Thus, the differential cross section contains a factor $|\psi_i(\mathbf{q})|^2$, where the momentum \mathbf{q} has a large component q_z directed along the momentum of the escaping electron and is close to it in magnitude, and two small components q_x and q_y , which depend on the angle between the electron and the photon beam. As a result, in general, the MD $|\psi_i(\mathbf{q})|^2$ cannot be studied in the most informative region of comparatively small momenta [$q \simeq (1-2)a_0^{-1}$, where a_0 is the Bohr radius or the atomic length unit] except for single crystals (see Section 4).

The electron momentum spectroscopy (EMS) considered in this review is the most informative microscopic technique, which allows one to obtain MDs for the individual occupied orbitals of a many-electron system (which differ in the binding energies) over the entire range of virtual electron momenta q , including their small values. The solution of this problem is the final aim of EMS, and this technique has no rivals in this respect. The investigation of MDs by the EMS technique reveals a variety of important physical properties of the objects under study, which are shortly listed below in paragraphs 1–9 and are discussed in detail in the next sections. The energy resolution of EMS is worse than that of PES: $\Delta E \simeq 0.2$ eV for gaseous targets, and $\Delta E \simeq 1$ eV for thin films. However, such a resolution proves to be sufficient for comparison, for example, of the MDs of individual electron orbitals in molecules and of the corresponding orbitals in complexes, analysis of MDs in different parts of the valence band in solids (including amorphous solids) and so forth. Of course, the EMS results obtained for the large virtual electron momentum q in a target coincide with those obtained by the PES technique [4].

The essence of the EMS technique proposed in papers [6–8] and first implemented about thirty years ago [9–11] is as follows. A gaseous or solid (very thin film) target is irradiated by a sufficiently monochromatic high-energy electron beam (the values of the electron energy E_0 required for different targets are given below). By means of a coincidence circuit, those events are separated from an abundance of events initiated by the electron beam in which the incident electron flying near one of the target electrons at a very small distance (on an atomic scale) ‘instantly’ knocks out the latter from the target through the Coulomb interaction and transfers to it a large part of the kinetic energy, which is usually chosen close to $E_0/2$.

In particular, if we consider the simplest case of coplanar geometry (the zero angle ϕ in Fig. 1a), then a coincidence circuit detects the ejected electrons with energies E_1 and E_2 , escaping at angles θ_1 and θ_2 to the direction of the incident beam (for $\theta_1 = \theta_2$ and $E_1 = E_2$, the kinematics is symmetric). In this way, the momenta \mathbf{p}_1 and \mathbf{p}_2 of the ejected electrons are determined. We mean, namely, the kinematics of quasi-elastic knock-out, which is close to the kinematics of free scattering when the angle between moments \mathbf{p}_1 and \mathbf{p}_2 is approximately 90° , and the energies E_1 and E_2 approach their values for free scattering. This restriction implies that the virtual momentum of the knocked-on electron $q \ll p_1, p_2$ and its binding energy in a target $|\varepsilon_{fi}| \ll E_1, E_2$. It is important that the momenta p_1 and p_2 are comparable to p_0 , i.e. energies E_1 and E_2 are comparable to E_0 .

The kinematics of the described binary collision are fixed with the EMS method in such a way that the effect of the many-electron system, in which the knocked-on electron finds

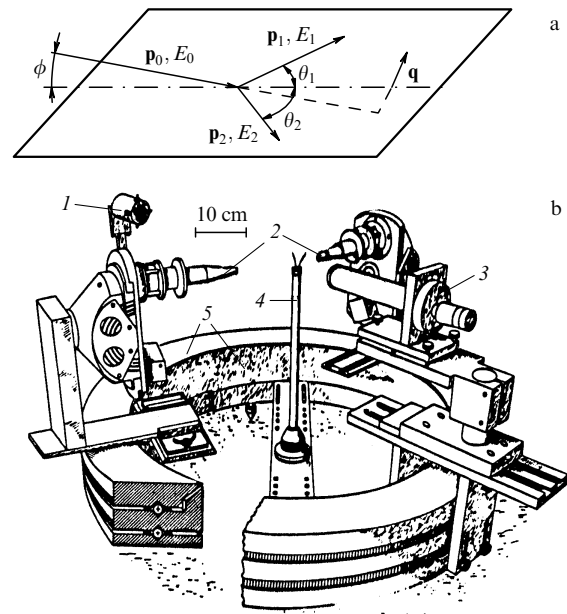


Figure 1. Schemes of (a) the (e, 2e) experiment, and (b) the (e, 2e) spectrometer: (1) Faraday trap, (2) electron analyzers, (3) electron gun, (4) gas beam of target atoms, (5) uncoupled rotary tables.

itself, is reduced to the fulfilment of two simple but principally important conditions: the knocked-on electron has a certain binding energy $\varepsilon_i < 0$ and (‘at the moment of impact’) the momentum $-\mathbf{q}$ (the momentum \mathbf{q} of the opposite direction is a recoil momentum transferred to the final system; such a choice of the momentum signs is traditional). These quantities are experimentally determined from the laws of conservation for binary collisions: $E_0 - \varepsilon_{fi} = E_1 + E_2$ and $\mathbf{p}_0 - \mathbf{q} = \mathbf{p}_1 + \mathbf{p}_2$. For this reason, the EMS technique is often called the (e, 2e) technique.

Thus, the quantities ε_{fi} and \mathbf{q} can be reconstructed from a small, reliably detectable deviation of the kinematics of the (e, 2e) process from the kinematics of fast-electron scattering by a free electron at rest. The momentum \mathbf{q} can be changed by slightly varying, for example, the escape angles of two ejected electrons (Fig. 1a). In this way, the MD of electrons in the orbital i with the binding energy ε_i is measured, which we denote as $|F_i(\mathbf{q})|^2$ (sometimes, this quantity is called the form factor). In so doing, the entire range of physically (and chemically) actual values of the momentum q , from zero up to several atomic units, may be covered. The noncoplanar kinematics when the angle ϕ in Fig. 1 is rather small are also methodically expedient; although, strictly speaking, upon deviation from the quasi-elastic impact geometry, a contribution of multiple scattering inside the interacting system begins building up.

The physical mechanism of the (e, 2e) process is very close to the Compton scattering of hard photons [12], however, in the latter case the accuracy of energy measurements is much worse than in the (e, 2e) method, so that, as upon annihilation of positrons, the total MDs of electrons are measured in the system under study.

In the last thirty years, the development of the experimental technique has gone through a number of stages related mainly to the type of spectrometers used [9–11, 13–21], the substantial increase in the rate of coincidence counting and in the accuracy of measurements of angles and energies of the

electrons flying apart. Geometry of the experimental setup depends on the target. In the case of atoms and molecules, the technique of crossed electron and gaseous target beams is employed (see Fig. 1b).

Electrostatic cylindrical-symmetry analyzers with two-dimensional position-sensitive detectors placed at their output are usually oriented at angles $\theta_1 = \theta_2 = 45^\circ$ to the direction of the electron beam or in the same plane with the beam ($\phi = 0$) or at a small angle ϕ to it. Initially, the coincidence circuit is adjusted, as a rule, for detection of electrons with equal energies ($E_1 = E_2$). The energy difference $E_0 - E_1 - E_2$ can be varied by continuously elevating the voltage across the electron gun, i.e. by increasing the energy E_0 of the electron beam.

The coincidence circuit detects a signal at some energy E_0 . This means that the difference $E_0 - E_1 - E_2 = \varepsilon_{fi}$, i.e. the ionization of electrons from the orbital i begins, accompanied by the ion transition to the final state f . Then, the electron-gun current is fixed and by varying angles θ_1 and θ_2 of the analyzers the angular dependence of the differential cross sections is obtained, which is used for constructing MDs of the ejected electrons.

The theoretical development of the (e, 2e) technique was concerned with fundamental problems of how the Coulomb short-range ee-correlations in many-electron systems are manifested in this technique [22], how the molecular electron orbitals are 'portrayed' (in particular, how the *sp*-hybridization is manifested) [23], and how the electron wave functions can be studied in a solid [24–28]. As a result, a great body of original data has been accumulated, which allows one to make a number of new conclusions concerning physical properties of quantum objects.

(1) It was shown experimentally [29–31] that according to the theoretical predictions the MDs of electrons are drastically different for atomic orbitals with different angular momenta l . This is of primary importance in analyzing the hybridization of orbitals in molecules and solids.

(2) The most direct method for studying the configuration interaction of the electrons in an atom, caused by short-range Coulomb ee-correlations, was proposed [22] and successfully implemented [29]. Along with the quasi-elastic knock-out, for example, of an electron from the He atom, when the He⁺ ion is mainly found in the ground $1s$ state, a weak satellite transition to the excited $2s$ and even the $3s$ state was studied, which reflects the admixture (with a small weight) of the $2s^2$ configurations, etc. to the ground state of the He atom. Similarly, mixing of the $2s^2$ and $2p^2$ configurations in the ground state of the Be atom results in the excitation of two ionic states, Be⁺($2s$) and Be⁺($2p$), in the (e, 2e) reaction [29]. In this case, the cross sections are proportional to the weights of these electronic configurations, and the corresponding MDs directly give 'portraits' of the $2s$ and $2p$ wave functions.

(3) The MDs of electrons in different orbitals were obtained with an energy resolution $\Delta E \simeq 1$ eV and momentum resolution $\Delta q \simeq 0.1a_0^{-1}$ for a variety of comparatively simple molecules, such as HF, N₂, H₂O, CO₂, NH₃, CH₄, C₂H₂, etc. (see Refs [31–33], where high-precision calculations of the wave functions are presented; the configuration interaction was considered in Refs [34, 35]). Notice that the (e, 2e) technique has a very high sensitivity to the type of *sp*-hybridization of the valence orbitals. It is shown that the use of more perfect wave functions (which only weakly affects the integral molecular properties such as the bond energy of a molecule, the spatial distribution of the total electron density,

etc.) substantially changes MDs for the outer electron orbitals and results in a quantitative agreement between the theory and experiment. A change in the type of *sp*-hybridization of the electron orbitals in the C, N, and O atoms composing above molecules was studied in detail depending on the molecular composition [31–33].

(4) It has been shown with a resolution of $\Delta E \simeq 0.5$ eV that the highest occupied (i.e. most weakly bound) molecular orbital (HOMO) substantially changes, being polarized upon complex formation [33]. This was demonstrated for trimethylamine (CH₃)₃N, which forms a loosely bonded complex (CH₃)₃N–BF₃ with boron trifluoride. The EMS was used to study HOMOs of dimetoximethane (CH₃O)₂CH₂ and glycine NH₂CH₂COOH [36], and the sensitivity of the form of these orbitals to the mutual arrangement of fragments (conformation) of a complex molecule was considered. It is known that HOMOs play a fundamental role in the formation of the molecular reactivity.

(5) The anisotropy of the electron MD was studied in the valence band of graphite single crystals [37–41]. The wave functions of the $2s$ and $2p$ oxygen orbitals were found from the (e, 2e) experiment by integrating the MDs over the energy of the corresponding bands in an ion Al₂O₃ polycrystal.

(6) The band structure of amorphous solid films of carbon, silicon, and germanium has been determined with a resolution of $\Delta E \simeq 1$ eV, and the corresponding wave functions have been studied [39, 42, 43]. The electron MDs in the valence band well demonstrate the existence of short-range order.

(7) Attempts were made to study a plasmaron satellite of the conduction band in metals by the (e, 2e) technique [44, 45]. However, only preliminary evidence for the existence of a plasmaron was obtained.

(8) The absolute cross sections for quasi-elastic knock-out of electrons from different shells of noble gas atoms were measured [15, 46–48], which allows one to check most reliably the theoretical models (plane wave approximation, distorted wave and eikonal approximations, etc.) and their validity depending on the electron beam energy.

(9) According to the theoretical recommendations [49–51], studies have been initiated (so far for atoms) of the (e, 3e) ionization with triple coincidences at initial energies of about several keV [52–54] and of the allied (γ , 2e) reaction with double coincidences [55–59], aiming to obtain the Fourier transforms of radial and angular ee-correlations in many-electron systems of different densities.

The above topics are considered in this review.

Notice that the role of the EMS technique in the physics and chemistry of many-electron systems is much more important than that in the physics of similar nuclear reactions (p, 2p), (p, pn) [60], (e, e'p) [61] and (p, p' α) [62]; the latter were used in papers [6, 7] as a primary example. The (p, 2p) technique, which requires particle beams with energies of several hundreds MeV, has efficient rivals in the nuclear spectroscopy of nucleons such as the stripping and pickup reactions (d, p), (p, d), (d, t), etc., which occur at considerably lower particle energies (10–40 MeV).

However, the study of the reactions (p, 2p), (p, pn), and (e, e'p) yielded an excellent result — the energies and unexpectedly large widths of the hole levels upon knocking out nucleons from deep shells of medium and heavy nuclei [60, 63]. The quasi-elastic ¹H(e, e' π^+)n reaction proceeding at the energy of several GeV was also successfully used for the study of the meson cloud in a nucleon [64].

We start the review with the theory of quasi-elastic knock-out of electrons from atoms [7], molecules [7, 23], and solids [7, 24]. In doing so we consider the most important variant of the theory, when a special choice of the high-energy beam and kinematics of quasi-elastic knock-out provides the simplest mechanism of the binary ee-interaction. As this takes place, a large energy and a large momentum are transferred to only one particle in the system, which gives in the most direct way valuable information on one-particle degrees of freedom in many-electron systems and on their coupling with collective motions.

We shall employ below the system of atomic units (au) because they are widely used in the scientific literature devoted to the (e, 2e) topic. Recall that the atomic unit of energy is 27.21 eV and the atomic unit of cross section is 27.98 Mb. In addition, we often use the generally adopted English abbreviations, such as TDCS, 5DCS, PWIA, DWIA, etc., which will be explained in the text when first appeared.

2. Theory of quasi-elastic knock-out of electrons at high energies

2.1 General formalism

We start from a general expression for the differential cross section in the collision theory, when in the final state there are two electrons in the continuum [65]:

$$d^4\sigma = \frac{2\pi}{p_0} |T_{fi}|^2 \delta(E_1 + E_2 + \varepsilon_{fi} - E_0) \frac{d\mathbf{p}_1}{(2\pi)^3} \frac{d\mathbf{p}_2}{(2\pi)^3}. \quad (2.1)$$

Here, \mathbf{p}_0 , \mathbf{p}_1 , and \mathbf{p}_2 are the momenta of the incident and two ejected electrons, respectively; E_0 , E_1 , and E_2 are their energies, and $\varepsilon_{fi} = \varepsilon_f - \varepsilon_i$ is the ionization potential of an atom in the i state with the wave function ψ_i , complying with the transition to the f state of the ion. If necessary, summation over the final and averaging over the initial states with the same quantum numbers should be made in Eqn (2.1).

In general, the amplitude T_{fi} of the reaction has a complicated structure corresponding to multiple scattering of the incident electron from atomic electrons and nucleus, which is described by the interaction potential

$$V = \sum_{s=1}^Z v_{0s} + V_0. \quad (2.2)$$

In the case of quasi-elastic knock-out of the atomic electron accompanied by transfer of a large momentum and energy to it, scattering of the incident electron proceeds via its single collision and is related to only one of the terms in the sum (2.2), for example, to v_{0z} , where z is the number of the knocked-on electron (the identity of electrons is taken into account below by the factor Z).

The amplitude in the quasi-elastic impact approximation [which is also called the plane wave impulse approximation (PWIA)] can be represented by the following diagram

$$T_{fi}^{\text{PWIA}} = \sum_{s=1}^Z$$

Since the theory of impulse approximation is well known [66], we will present the analytic expression for T_{fi}^{PWIA} without the derivation:

$$T_{fi}^{\text{PWIA}} = Z^{1/2} F_{fi}(\mathbf{q}) \langle \mathbf{p}_1, \mathbf{p}_2 | \hat{t}_{0z}(E_{\text{tot}} - \varepsilon_f) | \mathbf{p}_0, \mathbf{q} \rangle. \quad (2.3)$$

Here, the amplitude $F_{fi}(\mathbf{q})$ is the overlap integral

$$F_{fi}(\mathbf{q}) = \int \psi_i(\mathbf{r}_1, \dots, \mathbf{r}_z) \psi_f^*(\mathbf{r}_1, \dots, \mathbf{r}_{z-1}) \exp(i\mathbf{q}\mathbf{r}_z) d\mathbf{r}_1 \dots d\mathbf{r}_z, \quad (2.4)$$

where $\langle \hat{t}_{0z} \rangle$ is the Mott amplitude of the free ee-scattering stemming from the interaction v_{0z} .

Finally, we obtain the theoretical expression for the cross section which is measured in ‘coincidence’ experiments [6–8]:

$$\frac{d^4\sigma}{d\Omega_1 d\Omega_2 dE_1 dE_2} = \frac{Z p_1 p_2}{(2\pi)^3 p_0} \left(\frac{d\sigma}{d\Omega} \right)_{ee}^{\text{Mott}} |F_{fi}(\mathbf{q})|^2 \delta(E_1 + E_2 + \varepsilon_{fi} - E_0). \quad (2.5)$$

The cross section for the free Mott scattering has the form

$$\left(\frac{d\sigma}{d\Omega} \right)_{ee}^{\text{Mott}} = \frac{4}{Q^4} f(x) C(y), \quad (2.6)$$

where the following notation was used

$$f(x) = \frac{2\pi x}{\exp(2\pi x) - 1}, \quad C(y) = [1 + y^4 - y^2 \cos(2x \ln y)],$$

$$x = |\mathbf{p}_1 - \mathbf{p}_2|^{-1}, \quad y = \frac{|\mathbf{p}_0 - \mathbf{p}_1|}{|\mathbf{p}_0 - \mathbf{p}_2|}, \quad \mathbf{Q} = \mathbf{p}_0 - \mathbf{p}_1. \quad (2.7)$$

For high energies and large relative angles between ejected electrons, the cross section (2.6) is very close to the cross section for the elastic ee-scattering.

If necessary, averaging over the initial and summation over the final states with quantum numbers unobservable in the experiment should be performed in Eqn (2.5). In particular, expression (2.5) implies that the electron spins are not measured.

The square of the amplitude $F_{fi}(\mathbf{q})$ represents the electron MD in the atom corresponding to the $i \rightarrow f$ transition. The normalization of this distribution

$$S_{fi} = \int |F_{fi}(\mathbf{q})|^2 d\mathbf{q} \quad (2.8)$$

is called a spectroscopic factor. In an atom with unfilled electron shells, as in a nucleus [67], it characterizes the square of the so-called coefficient of fractional parentage [68].

In the Hartree–Fock (HF) approximation, the amplitude (2.4) takes the form $F_{fi}(\mathbf{q}) = S_{fi}^{1/2} \varphi_\gamma(\mathbf{q})$, where $\varphi_\gamma(\mathbf{q})$ is the wave function (in the momentum representation) of the one-particle orbital γ from which the electron is knocked out. The form factor $|F_{fi}(\mathbf{q})|^2$ can be treated as a correction factor to the Mott cross section, which reflects the peculiarities of electron ‘delocalization’ in a quantum target.

In a number of experimental papers [15, 46–48], the results of measurements of not only the MD shape for individual atoms were presented but also of the absolute cross sections, which yielded the limits of applicability of the above-discussed theory in the plane wave approximation. For the knock-out of an electron from the outer shells of such

atoms as Ne and Ar in the case of symmetric kinematics ($E_1 = E_2$), the inequality $E_0 > 2.5$ keV should hold (see Section 3).

2.2 Electron orbitals in molecules

In the case of molecules (and solids, see below) we arrive at the results [23] that no longer have an analog in the nuclear theory; however, some salient features of these results common with those in the theory of X-ray scattering, Compton scattering of photons [69], etc. can be noted, namely, the interference of the amplitudes of quasi-elastic knock-out of electrons from different centers.

Expression (2.4) can be simply generalized to the case of molecules:

$$F_{fi}(\mathbf{q}) = \int \exp(i\mathbf{q}\mathbf{r}_z) \psi_f^*(\mathbf{r}_1, \dots, \mathbf{r}_{z-1}; \mathbf{R}_1, \dots, \mathbf{R}_N) \times \psi_i(\mathbf{r}_1, \dots, \mathbf{r}_z; \mathbf{R}_1, \dots, \mathbf{R}_N) d\mathbf{r}_1 \dots d\mathbf{r}_z d\mathbf{R}_1 \dots d\mathbf{R}_N, \quad (2.9)$$

where $\mathbf{R}_1, \dots, \mathbf{R}_N$ are the coordinates of nuclei in the laboratory reference frame. By using the adiabatic approximation, we transform this expression to the form

$$F_{fi}(\mathbf{q}) = \int d\Omega \psi_{J'M'K'}^* \text{rot}(\Omega) \psi_{JMK} \text{rot}(\Omega) \times \int \prod_{\alpha} dQ_{\alpha} \psi_{v'}^* \text{vib}(Q_{\alpha}) \psi_v \text{vib}(Q_{\alpha}) \times \int \prod_{i=1}^z d\mathbf{r}_i \exp(i\mathbf{q}\mathbf{r}_z) \psi_{n'}^* \text{el}(\mathbf{r}_1, \dots, \mathbf{r}_{z-1}; Q_{\alpha}) \psi_n \text{el}(\mathbf{r}_1, \dots, \mathbf{r}_z; Q_{\alpha}), \quad (2.10)$$

where primed subscripts correspond to the final state, and the vectors \mathbf{Q}_{α} form a system of normal coordinates of the molecule whose orientation in the laboratory frame is specified by the Eulerian angles Ω .

Taking into account, as usual, the equilibrium positions of nuclei in the electron wave functions ψ_n^{el} and $\psi_{n'}^{\text{el}}$ and one-particle HF wave functions $\psi_{\gamma}(\mathbf{r}; \mathbf{R}_s)$ of orbitals γ , we obtain the following expansion for the electronic part of a molecular wave function

$$\psi_n^{\text{el}}(\mathbf{r}_1, \dots, \mathbf{r}_z; \mathbf{R}_s) = \sum_{n'', \gamma} \langle n|n'', \gamma \rangle \psi_{n''}^{\text{el}}(\mathbf{r}_1, \dots, \mathbf{r}_{z-1}; \mathbf{R}_s) \psi_{\gamma}(\mathbf{r}_z; \mathbf{R}_s), \quad (2.11)$$

where $\langle n|n'', \gamma \rangle$ are the coefficients of fractional parentage. Considering (2.11), the momentum amplitude (2.10) is transformed to

$$F_{fi}(\mathbf{q}, \mathbf{R}_s) = g_{vv'} \int d\Omega \psi_{J'M'K'}^* \text{rot}(\Omega) \psi_{JMK} \text{rot}(\Omega) F_{m'm'}^{\text{el}}(\mathbf{q}, \mathbf{R}_s). \quad (2.12)$$

The quantity \mathbf{R}_s in Eqns (2.11) and (2.12) stands for a set of nuclear radius vectors which are now parameters

$$F_{m'm'}^{\text{el}}(\mathbf{q}, \mathbf{R}_s) = \langle n|n'', \gamma \rangle \int \exp(i\mathbf{q}\mathbf{r}) \psi_{\gamma}(\mathbf{r}, \mathbf{R}_s) d\mathbf{r}, \quad (2.13)$$

$$g_{vv'} = \int \prod_{\alpha} dQ_{\alpha} \psi_{v'}^* \text{vib}(Q_{\alpha}) \psi_v \text{vib}(Q_{\alpha}), \quad \sum_{v'} |g_{vv'}|^2 = 1. \quad (2.14)$$

Assuming that the molecules under study are in the ground state and are characterized by a thermal distribution over the rotational states with the temperature

$$T \gg T_{\text{rot}} (T_{\text{rot}} = h^2/8\pi^2 kI),$$

we can use the property of completeness of the rotational wave functions

$$\sum_{JMK} \psi_{JMK}^* \text{rot}(\Omega') \psi_{JMK} \text{rot}(\Omega) = \delta(\Omega - \Omega').$$

Then, the MD averaged over the rotational states takes the form

$$\overline{|F_{\gamma}(q, \mathbf{R}_s)|^2} = \sum_{v'} |g_{0v'}|^2 \int \frac{d\Omega}{8\pi^2} |F_{0n'}^{\text{el}}(\mathbf{q}, \mathbf{R}_s)|^2 = \sum_{v'} |g_{0v'}|^2 \langle 0 | n', \gamma \rangle \left| \int \frac{d\Omega}{4\pi} \exp(i\mathbf{q}\mathbf{r}) \psi_{\gamma}(\mathbf{r}; \mathbf{R}_s) d\mathbf{r} \right|^2, \quad (2.15)$$

i.e. the result is averaged over orientations of the vector \mathbf{q} with fixed spatial orientation of the molecule, as in the theory of X-ray scattering.

Let us represent the molecular orbital ψ_{γ} as a linear combination of atomic orbitals (MO LCAO):

$$\psi_{\gamma}(\mathbf{r}; \mathbf{R}_s) = \sum_{s=1}^N \sum_{p=1}^{K_s} C_p^s(\gamma) \varphi_p^s(\mathbf{r}_s), \quad \mathbf{r}_s = \mathbf{r} - \mathbf{R}_s, \quad (2.16)$$

where K_s is the basis set dimensionality of the atom s , and the coefficients C_p^s characterize the hybridization properties of the atomic orbitals. The individual components $\varphi_p^s(\mathbf{r})$ are the Coulomb wave functions $\varphi_{nlm}(\mathbf{r})$ with the Fourier transform

$$\varphi_{nlm}(\mathbf{q}) = \int \varphi_{nlm}(\mathbf{r}) \exp(i\mathbf{q}\mathbf{r}) d\mathbf{r} \equiv P_{nl}(q) Y_{lm}(\Omega_q).$$

Substitution of expression (2.16) into (2.15) gives

$$\overline{|F_{\gamma}(q, \mathbf{R}_s)|^2} = G \int \frac{d\Omega_q}{4\pi} \left| \sum_{s=1}^N \exp(i\mathbf{q}\mathbf{R}_s) \sum_{p=1}^{K_s} C_p^s(\gamma) \varphi_p^s(\mathbf{q}) \right|^2, \quad G = \sum_{v'} |g_{0v'}|^2 \langle 0 | n', \gamma \rangle^2. \quad (2.17)$$

We shall obtain the final expression for the form factor (2.17) in two variants. The first one is based on the expansion of $\exp\{i\mathbf{q}(\mathbf{R}_s - \mathbf{R}_{s'})\}$ in (2.17) in terms of the partial waves [23], which yields

$$\overline{|F_{\gamma}(q, \mathbf{R}_s)|^2} = \overline{F_{\text{at}}^2} + \overline{F_{\text{int}}^2}. \quad (2.18)$$

Here, the following designations were used:

$$\overline{F_{\text{at}}^2} = \frac{G}{4\pi} \sum_{s=1}^N \sum_{p,p'}^{K_s} C_p^s(\gamma) C_{p'}^{*s}(\gamma) |P_{n_l l_i}(q)|^2 \delta_{l_i l_i'} \delta_{m_i m_i'},$$

$$\overline{F_{\text{int}}^2} = 2G \text{Re} \sum_{s' > s} \sum_{p=1}^{K_s} \sum_{p'=1}^{K_{s'}} C_p^s(\gamma) C_{p'}^{*s'}(\gamma) P_{n_l l_i}(q) P_{n_{l'} l_{i'}}^*(q) \times \sum_{l=|l_i-l_{i'}|}^{l_i+l_{i'}} i^l j_l(q|\mathbf{R}_s - \mathbf{R}_{s'}|) (-1)^{m_i} \sqrt{\frac{(2l+1)(2l_i+1)(2l_{i'}+1)}{4\pi}} \times Y_{l, m_i - m_{i'}}(\Omega_{\mathbf{R}_s - \mathbf{R}_{s'}}) \begin{pmatrix} l & l_i & l_{i'} \\ m_i & -m_i & -m_{i'} \end{pmatrix} \begin{pmatrix} l & l_i & l_{i'} \\ 0 & 0 & 0 \end{pmatrix},$$

where $j_l(qR)$ is the spherical Bessel function, $i \equiv (s, p)$, and the rest of the notation is obvious. Expression (2.18) is probably the most convenient for diatomic and polyatomic molecules with a simple symmetry of the CH_4 type [23].

As an example, consider the σ_g orbital of a diatomic molecule (with atoms a and b) with hybridization from the s and p orbitals:

$$\begin{aligned}\psi_{g\sigma} &= C_s(|ns_a\rangle + |ns_b\rangle) + C_p(|n'p\sigma_a\rangle - |n'p\sigma_b\rangle), \\ \overline{|F|_{\text{at}}^2} &= \frac{G}{2\pi} \left[C_s^2 |P_{n0}(q)|^2 + C_p^2 |P_{n'1}(q)|^2 \right], \\ \overline{|F|_{\text{int}}^2} &= \frac{G}{2\pi} \left[2C_s^2 |P_{n0}(q)|^2 j_0(qR) - C_p^2 |P_{n'1}(q)|^2 \right. \\ &\quad \left. \times \{j_0(qR) - 2j_2(qR)\} + 2\sqrt{3} C_s C_p P_{n0}(q) P_{n'1}(q) j_1(qR) \right].\end{aligned}$$

Here, we used the following identities:

$$\sum_{J'} (2J' + 1) \begin{pmatrix} J' & l & J \\ 0 & 0 & 0 \end{pmatrix}^2 = 1, \quad 2 \sum_{l \text{ even}} (2l + 1) j_l^2\left(\frac{x}{2}\right) = 1 + j_0(x).$$

In the HF approximation for the σ orbital occupied by two electrons, $\langle 0|n', \gamma^2\rangle$ is equal to 2, while for the π orbital it equals 4. This example shows that MDs give an easily interpretable direct ‘portrait’ of individual valence orbitals, which is highly sensitive to the type of sp -hybridization.

The second variant is based on the expansion of $\exp(i\mathbf{q}\mathbf{R}_s)$ in (2.17) in terms of the partial waves [23]:

$$\begin{aligned}\overline{|F_\gamma(q, \mathbf{R}_s)|^2} &= G \sum_{s, s'} \sum_{p=1}^{K_s} \sum_{p'=1}^{K_{s'}} C_p^s(\gamma) C_{p'}^{s'}(\gamma) P_{n_i l_i}(q) P_{n_i' l_i'}^*(q) \\ &\quad \times (-1)^{m_i'} \sqrt{(2l_i + 1)(2l_i' + 1)} \sum_{lm} \sum_{l'm'} l' m' (-i)^l i^{l'} j_l(qR_s) \\ &\quad \times j_{l'}(qR_{s'}) ; Y_{lm}(\Omega_{\mathbf{R}_s}) Y_{l'm'}^*(\Omega_{\mathbf{R}_{s'}}) (-1)^m \sqrt{(2l + 1)(2l' + 1)} \\ &\quad \times \sum_{LM} (-1)^M (2L + 1) \begin{pmatrix} l & l_i & L \\ -m & m_i & M \end{pmatrix} \begin{pmatrix} l & l_i & L \\ 0 & 0 & 0 \end{pmatrix} \\ &\quad \times \begin{pmatrix} l' & l_i' & L \\ m' & -m_i' & -M \end{pmatrix} \begin{pmatrix} l' & l_i' & L \\ 0 & 0 & 0 \end{pmatrix}.\end{aligned}\quad (2.19)$$

Because Eqn (2.19) immediately contains vectors \mathbf{R}_s , the symmetry properties of the molecule are explicitly represented, although this expression is more cumbersome than (2.18). A wide application of the above expressions is discussed in Section 4.

2.3 Electron wave functions in a solid

The electron wave function in a single crystal in the tight-binding approximation possesses translation invariance and has the form

$$\psi_{\mathbf{k}\lambda}(\mathbf{r}) = \frac{1}{\sqrt{N}} \sum_{\mathbf{R}} \exp(i\mathbf{k}\mathbf{R}) \varphi_\lambda(\mathbf{r} - \mathbf{R}).\quad (2.20)$$

Here, \mathbf{k} is the quasi-momentum related to the first Brillouin zone, \mathbf{R} is the cell coordinate, λ is the zone index corresponding to the atomic wave functions $\varphi_\lambda(\mathbf{r})$, and N is the number of atoms in the crystal. The Fourier amplitude (2.4) for (2.20) can be written in the form

$$\begin{aligned}F_{\mathbf{k}\lambda}(\mathbf{q}) &= \frac{1}{\sqrt{N}} \varphi_\lambda(\mathbf{q}) \sum_{\mathbf{R}} \exp\{i(\mathbf{k} - \mathbf{q})\mathbf{R}\} \\ &= \sqrt{N} \varphi_\lambda(\mathbf{q}) \sum_{\mathbf{B}} \delta_{\mathbf{k}+\mathbf{B}, \mathbf{q}},\end{aligned}\quad (2.21)$$

where \mathbf{B} is the reciprocal lattice vector. By this means the cross section is described by the expression [7, 24]

$$\begin{aligned}\frac{d^4\sigma}{d\Omega_1 d\Omega_2 dE_1 dE_2} &= \frac{p_1 p_2 g}{(2\pi)^3 p_0} \sum_{\mathbf{B}} |\varphi_\lambda(\mathbf{q})|^2 N \delta_{\mathbf{k}+\mathbf{B}, \mathbf{q}} \\ &\quad \times \left(\frac{d\sigma}{d\Omega} \right)_{\text{ee}}^{\text{Mott}} \delta(E_1 + E_2 - \varepsilon_\lambda(\mathbf{k}) - E_0).\end{aligned}\quad (2.22)$$

Here, it should be taken into account that $NV\delta_{\mathbf{q}, \mathbf{k}} = (2\pi)^3 \delta(\mathbf{q} - \mathbf{k})$, where V is the volume per atom. The factor g in Eqn (2.22) is equal to the number of valence electrons per atom; for brevity, we assume it equal to unity at a later time.

For fixed $\varepsilon_\lambda(\mathbf{k}) = -E_0 + E_1 + E_2$, by varying \mathbf{q} in the specified direction in a single crystal (which can be done by the EMS technique), we obtain the $|F_{\mathbf{k}\lambda}(\mathbf{q})|^2$ MD in the form of a discrete set of peaks corresponding to different \mathbf{B} , where \mathbf{k} is specified by the energy $\varepsilon_\lambda(\mathbf{k})$. By continuously varying the value of $E_1 + E_2$, and thereby $\varepsilon_\lambda(\mathbf{k})$ and \mathbf{k} , we obtain the entire dependence $|\varphi_\lambda(\mathbf{q})|^2$ in the first Brillouin zone ($\mathbf{B} = 0$) (see discussion below about Al_2O_3 polycrystals).

Despite its compactness, expression (2.22) is quite informative and allows one to analyze in detail the interesting experimental data and also (as one of the theoretical proposals) to consider various manifestations of the sd -hybridization of the electron wave functions in the conduction band of a copper single crystal [24], which in turn suggests that the (e, 2e) technique can be successfully used for studying the electronic structure of high-temperature superconductors (see Refs [25–28], where the theoretical discussion about other aspects of the band structure relevant to the (e, 2e) technique is of interest).

Consider the influence of collective effects on one-particle degrees of freedom using the one-particle Green functions. For this purpose, we represent expression (2.4) in the form

$$\begin{aligned}F_{\alpha f}(\mathbf{q}) &= \int \exp(i\mathbf{q}\mathbf{r}_N) \psi_{\alpha f}^*(1, \dots, N-1) \\ &\quad \times \psi_0(1, \dots, N) d\tau_1 \dots d\tau_N \equiv \frac{1}{\sqrt{N}} S_{\alpha f} \varphi_\alpha(\mathbf{q}).\end{aligned}\quad (2.23)$$

Here, $S_{\alpha f}$ is the spectroscopic factor, and the function $\varphi_\alpha(\mathbf{q})$ is normalized to unity. The Slater determinant ψ_0 can be written as an identity [70]

$$\psi_0(1, \dots, N) \equiv \frac{1}{\sqrt{N}} \sum_i \varphi_i(N) \hat{a}_i |0\rangle,$$

where i denotes the electronic state, \hat{a}_i is the electron annihilation operator, and $|0\rangle \equiv \psi_0$. In this case, expression (2.23) takes a compact form

$$F_{\alpha f}(\mathbf{q}) = \frac{1}{\sqrt{N}} \varphi_\alpha(\mathbf{q}) (\hat{a}_\alpha)_{0f}.\quad (2.24)$$

Note that for plane waves one obtains $\varphi_{\mathbf{k}}(\mathbf{q}) = \delta(\mathbf{k} - \mathbf{q})$.

Let us introduce the spectral density of the one-particle Green function [71]

$$A(\mathbf{q}, \varepsilon) = \sum_f |(\hat{a}_\mathbf{q})_{0f}|^2 \delta(\varepsilon - \varepsilon_f)\quad (2.25)$$

in such a way that

$$A^0(\mathbf{q}, \varepsilon) = \delta(\varepsilon - [\varepsilon_q - \mu])$$

for the Fermi gas of noninteracting electrons. The quantity

$$n(\mathbf{q}) = \int_{-\infty}^0 A(\mathbf{q}, \varepsilon) d\varepsilon$$

characterizes the total electron MD in a solid, and the difference of the function $n(\mathbf{q})$ from the step function $\Theta(q - k_F)$ is the simplest manifestation of the deviation of a degenerate electron gas from an ideal gas. Comparison of Eqn (2.25) with (2.23) and (2.24) shows that the function $A(\mathbf{q}, \varepsilon)$ is equivalent to the quantity $\sum_f S_{\alpha f}^2 |\varphi_{\alpha}(\mathbf{q})|^2$ applied to a unit energy interval. Now, we can write out the expression for the cross section [25, 26]

$$\frac{d^4\sigma}{d\Omega_1 d\Omega_2 dE_1 dE_2} = \frac{p_1 p_2}{(2\pi)^3 p_0} \left(\frac{d\sigma}{d\Omega_1} \right)_{cc}^{Mott} \times C_{\sigma}^2 A(\mathbf{q}, \varepsilon) \delta(E_1 + E_2 - \varepsilon - E_0), \quad (2.26)$$

where the spectroscopic factor C_{σ}^2 characterizes the spin degeneration. A formula equivalent to (2.26) is used in nuclear physics [72] for the analysis of results of the (e, e'p) reaction at the energy $E_0 \simeq 600$ MeV for medium and heavy nuclei [61], when the density of levels of the final nucleus is high.

One can see from Eqn (2.26) that the (e, 2e) technique allows one to study the entire 'topography' of the spectral density $A(\mathbf{q}, \varepsilon)$ — its dependence both on \mathbf{q} and ε . This topography just reveals the role of collective effects.

As an example, consider the knock-out of an electron from the closed shell of an atom in metal ('the deep hole'). In this case, the collective response of the conduction electrons to a 'sudden' appearance of a deep hole is of interest [25, 26]. Two simplifying circumstances become important. First, the deep hole does not multiply (in contrast to the soft particle-hole excitations of the Fermi gas), and its recoil momentum can be neglected ('an infinitely heavy ion'). Second, the momentum of collective excitation is small compared to the mean value of q for a highly bound electron.

Thus, the factor taking into account the formation of a deep hole α is simply introduced as a separate multiplier, and the momentum amplitude (2.24) can be presented in the form

$$F_{\alpha f}(\mathbf{q}) = C_{\sigma}(\hat{a}_{\alpha})_{0f} \varphi_{\alpha}(\mathbf{q}),$$

so that the cross section is

$$\frac{d^4\sigma}{d\Omega_1 d\Omega_2 dE_1 dE_2} = \frac{p_1 p_2}{(2\pi)^3 p_0} \left(\frac{d\sigma}{d\Omega_1} \right)_{cc}^{Mott} \times S_{\alpha}^2 Z_{\alpha}(\varepsilon) |\varphi_{\alpha}(q)|^2 \delta(E_1 + E_2 - \varepsilon - E_0),$$

where

$$Z_{\alpha}(\varepsilon) = \sum_f |(\hat{a}_{\alpha})_{0f}|^2 \delta(\varepsilon - \varepsilon_f) \quad (2.27)$$

is the spectral density of the deep hole [73], with summation being performed over the excited states of a system of conduction electrons, and $S_{\alpha}^2 = 2(2l + 1)$.

In the theory of collective response [73], the function $Z_{\alpha}(\varepsilon)$ has the form

$$Z_{\alpha}(\varepsilon) = \sum_n \left(\exp(-a) \frac{a^n}{n!} \right) A(\varepsilon - \varepsilon_0 - n\omega_p). \quad (2.28)$$

Here, $A(x) \sim |x|^{-(1-\beta)} \Theta(x)$, $\beta = 2 \sum (2l + 1) (\delta_l/\pi)^2$, $a \simeq r_s/6$, δ_l are the phases of an electron scattering by the deep hole potential, r_s is the mean distance between conduc-

tion electrons, and ω_p is the plasmon energy (for brevity, its dispersion is not discussed).

Consider the term with $n = 0$ in Eqn (2.28) (the main peak without plasmon satellites). Calculations have shown [73] that for such metals as Li, Na, and Cu the values of $1 - \alpha$ are equal to 0.80, 0.87, and 0.98, respectively, i.e. the (e, 2e) cross section should exhibit the Mahan–Nozieres threshold singularity for $\varepsilon \rightarrow \varepsilon_0$ in the form of a sharp asymmetric peak [25, 26]. At the same time, the result will be different for the threshold UV absorption, which was considered in papers [73] as a physical application of the theory of collective response. Instead of $A(\varepsilon)$, the quantity $B(\omega) \sim |\omega|^{-\beta_l}$ appears in (2.28), where $\beta_l = 2(\delta_l/\pi) - \beta$, $\omega = \varepsilon - \varepsilon_0$, and l is the orbital moment of an electron on the Fermi surface after its transition from the highly bound state.

If $1 - \beta > 0$, but $\beta_l < 0$ (for example, upon the s - p transition in Li, Na and some other metals, where $\beta_l \simeq -0.1$ [73, 74]), the Mahan–Nozieres singularity manifests itself upon optical absorption as the threshold suppression of the cross section. The physical reason is that the singularities reveal themselves not in the function $Z(\varepsilon)$ for the deep hole but in the spectral density $B(\omega)$ of a convolution of the deep-hole Green function with the Green function of the conduction electron upon the action of the nonstationary potential of the deep hole. This is one of numerous examples when the (e, 2e) technique can give substantially new information on the object under study (in contrast to optical methods), and the energy resolution achieved at present allows one to perform such experiments (see below).

Another example of the study on the spectral density $A(\varepsilon, \mathbf{q})$ by means of the (e, 2e) technique is an investigation of the plasmaron satellite in the conduction band in metals. The spectral density $A(\varepsilon, \mathbf{q})$ of the ideal Fermi gas as a function of ε at \mathbf{q} fixed is zero everywhere except the energy $\varepsilon = \varepsilon_0 - (k_F^2 - q^2)/2m^*$, where a peak of the unit intensity shows up. For a real electron gas, for example, in a thin Mg film ($r_s = 3$), the calculation performed by the random phase method [75] yields two peaks near the bottom of the conduction band (say, at $q = 0.2 k_F$). These peaks have comparable heights: one of them, with intensity 0.6, is located approximately where the unit peak is observed in the ideal Fermi gas, and the second one, with intensity 0.35, is located $1.5 \omega_p$ below the bottom of the conduction band ($\omega_p \simeq 17$ eV). The second peak is caused by the collective excitation, i.e. a plasmaron. Its characteristic feature is that the limiting momentum q_{\max} above which the hole level broadens (gets wider) approximately equals $0.5 k_F$ [75]. This property can be conveniently studied namely by the (e, 2e) technique. It allows one to separate 'trivial' events, when an electron is knocked out from the conduction band and excites a plasmon 'in the external way' during propagation through a film. Experimental studies [44, 45] have given only preliminary evidence of the existence of a plasmaron because of the insufficient statistical accuracy.

Having reported the fundamentals of the formalism, we can enter into a discussion of the results obtained for atoms, molecules and solids.

3. Electron momentum spectroscopy of atoms

3.1 Atoms as a bridge to quantum chemistry

The EMS was mainly applied to atoms of noble gases He, Ne, Ar, Xe, and Kr. The EMS kinematics of noble gases have

been extensively studied by Australian and Italian scientists, so we refer here to reviews [76–79] which contain references to the original papers.

The EMS language is the language of HF orbitals, and only in the case of light atomic particles (H, He, H[−], Li, etc.) it seems timely to use the language of the quantum theory of few-body systems. In fact, we are dealing with different approximate models of the same physical reality, the difference being that the HF model considers a part of the ee-interaction implicitly in the mean-field potential, while another part of this interaction is explicitly specified in the wave function of an atom (residual ion) by including the interaction of several electronic configurations (the so-called correlation effects).

Theoretical models of systems containing few particles assume either the direct numerical solution of the initial Schrödinger equation or the use of trial functions taking into account their radial and angular correlators, when the explicit dependence on the coordinate \mathbf{r}_{12} is introduced into the wave function. For example, for para helium the trial wave function of the ground 1S_0 state, allowing for the interaction of electron configurations (1s, 1s), (1s, 2s), (2s, 2s), (2p, 2p), etc., can be used or the Hilleraas type function [see Eqn (3.12)]. Of course, these representations are related to each other and, for example, the Hilleraas function can always be expanded over a total system of one-particle HF wave functions, although the number of significant terms in this expansion can be large.

In this section, we shall use the language of interaction of the HF configurations when discussing (by the example of the He atom) the important question of how the wave functions of many-electron systems differ from the HF wave functions (or how the ee-correlations manifest themselves in these systems). Then we apply the theory of few-body systems to the He atom.

After an ‘instant impact’, a virtual state of an atom with a hole is formed, which should decay to the ion state with the same binding energy; we denote this state by a subscript α . The summation in expression (2.5) for the cross section should be performed over this subscript. Let us write the initial state of the atom as a product of the wave function of the atomic orbital from which ionization occurs and the residual minor

$$|\psi_i\rangle = \frac{1}{\sqrt{Z}} \sum |\phi_{nl} \Phi_i^R\rangle. \quad (3.1)$$

The number of terms in the sum corresponds to the number of electrons in the system.

The ion state can be written for generality in the representation of interacting electron configurations:

$$\langle\psi_{f_z}| = a_{\alpha 0} \langle\phi_{f_z}^{\text{HF}}| + \sum_j a_{\alpha j} \langle\Phi_{f_z}^j|. \quad (3.2)$$

Here, $\langle\Phi_{f_z}^j|$ are the electron configurations that, in our opinion, should be present in the ion model. According to the Brillouin theorem, they include two or more excited electrons in order to correspond to the same quantum numbers as the $|\phi_{f_z}^{\text{HF}}\rangle$ state.

The convolution of (3.1) and (3.2) yields

$$F_{f_z i}(q) = \sum \phi_{nl}(q) \left[a_{\alpha 0} \langle\phi_{f_z}^{\text{HF}}|\Phi_i^R\rangle + \sum_j a_{\alpha j} \langle\Phi_{f_z}^j|\Phi_i^R\rangle \right]. \quad (3.3)$$

The role of the sum taken over the number of electrons in the orbital in Eqn (3.3) after substitution in Eqn (2.5) and averaging over the initial states is reduced to a simple replacement of the factor Z in the cross section by the number of electrons in the orbital N_{nl} . In turn, the square of the quantity in brackets in Eqn (3.3) is equal to the spectroscopic factor $S_{f_z i}$ considered in Section 2.1. Notice that the convolution $\langle\phi_{f_z}^{\text{HF}}|\Phi_i^R\rangle$ is not equal to unity because radial one-particle wave functions of an atom and an ion are generally different [80]. The convolutions in the sum over j can be either zero due to the orthogonality of the angular states (as in the case of inert gases) or can make, as a rule, a small contribution in the case of a weakly populated outer electron shell.

Of course, other expansions of the initial and final states are possible depending on the physical properties of an atomic target and an ion; however, the form factor (3.3) will contain in any case (in the configuration interaction approximation) the Fourier transform of the one-particle wave function of the atomic orbital from which the ionization has occurred. This orbital is identified by the dependence of the differential cross section on q and by the difference energy spectrum $\varepsilon_{\alpha f} = -E_0 + E_1 + E_2$.

Figure 2 shows the classical angular spectra in the case of the (e, 2e) ionization from the 2s and 2p shells of the Ne atom.

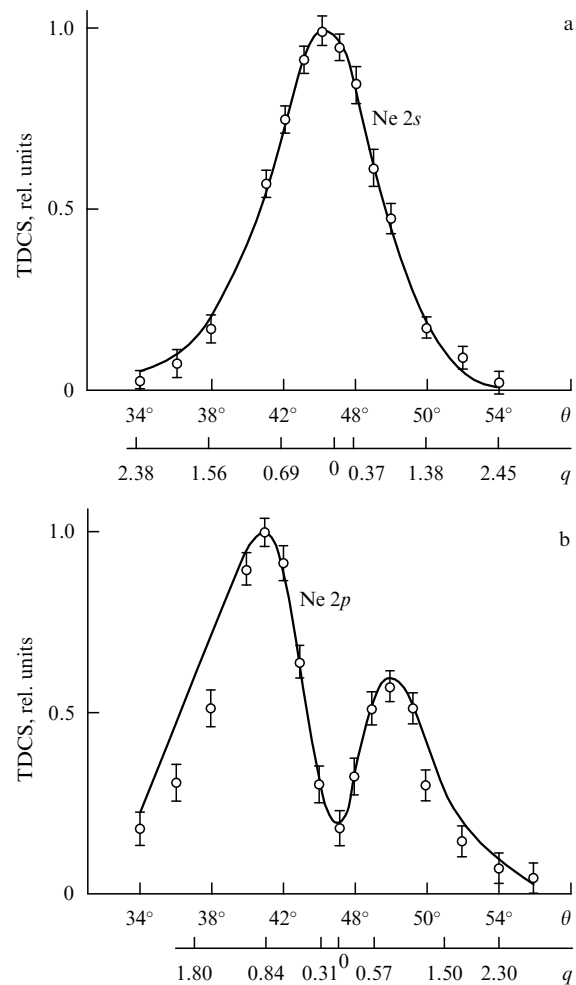


Figure 2. Classical angular and momentum TDCSs for the Ne(e, 2e)Ne⁺ reaction upon the (e, 2e) ionization from the (a) s and (b) p shell; $E_0 = 2.6$ keV [78].

The qualitative difference in the shapes of the curves of triple differential cross sections (TDCS) clearly demonstrates the advantage of EMS, which allows one to separate with high accuracy the contributions of the s and p components when studying the hybridized orbitals in quantum chemistry, and also to reliably distinguish the MDs of σ_u and σ_g orbitals in diatomic molecules (N_2 , F_2 , etc.). For smaller angles in the case of the p shell, the result of calculations with trial functions taken from the handbook [80] does not well agree with experiment. This can be explained by the necessity of accounting for a small correlation between the $2s$ and $2p$ configurations in the Ne atom, as was pointed out in Ref. [81].

Of great interest is a series of symmetric relativistic experiments on the ionization of the k shells in Cu, Ag, and Au atoms [82]. The correlation effects are not very important for deep holes, so that the mechanism of ionization of the k shells of heavy atoms is similar to that of the He ionization. However, in this case the relativistic effects and the extra-energetic effects due to distortion of plane waves play an important role, the latter emerging from the fact that these waves spend a 'long time' in the mean atomic field. Simple estimates have shown that this assumption is correct [83]. It has received further support through relativistic calculations in the distorted wave impulse approximation (DWIA) [84].

To describe the details, however, the complete relativistic calculations were required, taking into account the quantum electrodynamic propagator, spin-orbital effects, singlet and triplet states and discarding the amplitude factorization. It became obvious that the quasi-relativistic approach does not work. Also, it was apparent that calculations of the distorted waves should take into consideration the excitation channels along with elastic scattering channels. These circumstances impose natural restrictions on the fields of applicability of the PWIA [see Eqn (2.3)] in the case of atomic ionization from the inner shells: by increasing energy, we pass to the relativistic domain, where the elegant formula (2.5) is not valid. Other restrictions are considered in Section 3.3.

Consider anew the correlation effects and their influence on the energy and angular spectra. If the configuration interaction in the initial-state wave function is strong, representation (3.2) should be used not only for an ion but for a target as well. In this case, contributions from the MDs of orbitals with different angular momenta can make their appearance in expression (3.3), for example, the s and p orbitals, which will affect both the energy and momentum (angular) spectra of the $(e, 2e)$ reactions. In particular, along with the peaks related to the dominating HF orbitals, the energy spectrum will exhibit (in the case of an adequate resolution) the corresponding correlation peaks — satellites of the main peaks of the different intensity (Fig. 3). This conclusion was drawn by Levin in paper [22], where the energy and angular spectra of the C and Be atoms were calculated taking into account the intense configuration interaction in the ground state.

Beryllium is of interest because it is similar to the He atom: along with the filled inner shell, it also contains two outer-shell electrons. The ground 1S_0 state is a superposition of two electron configurations $0.95(1s^22s^2) + 0.32(1s^22p^2)$. It can transfer either to the 2S state of the Be^+ ion (the $1s^22s$ configuration, the transition energy $\varepsilon_{fi} = 9.3$ eV) or the 2P state (the $1s^22p$ configuration, $\varepsilon_{fi} = 13.3$ eV). In contrast to He, the electronic states of the Be^+ ion are quasi-degenerate because the energies of transitions to these states are different, and the energy $(e, 2e)$ spectrum exhibits an additional correlation peak. As in the case of helium, the P form factor is approximately 100 times smaller than the S form factor; however, as a whole the distributions correspond to those displayed in Fig. 2.

3.2 Helium as the simplest target

Helium is a simplest two-electron target which permits in a number of cases the study (within the framework of three- and four-particle microscopic models) of the mechanisms of $(e, 2e)$ and $(e, 3e)$ collisions and the effect of the ee -correlations on the

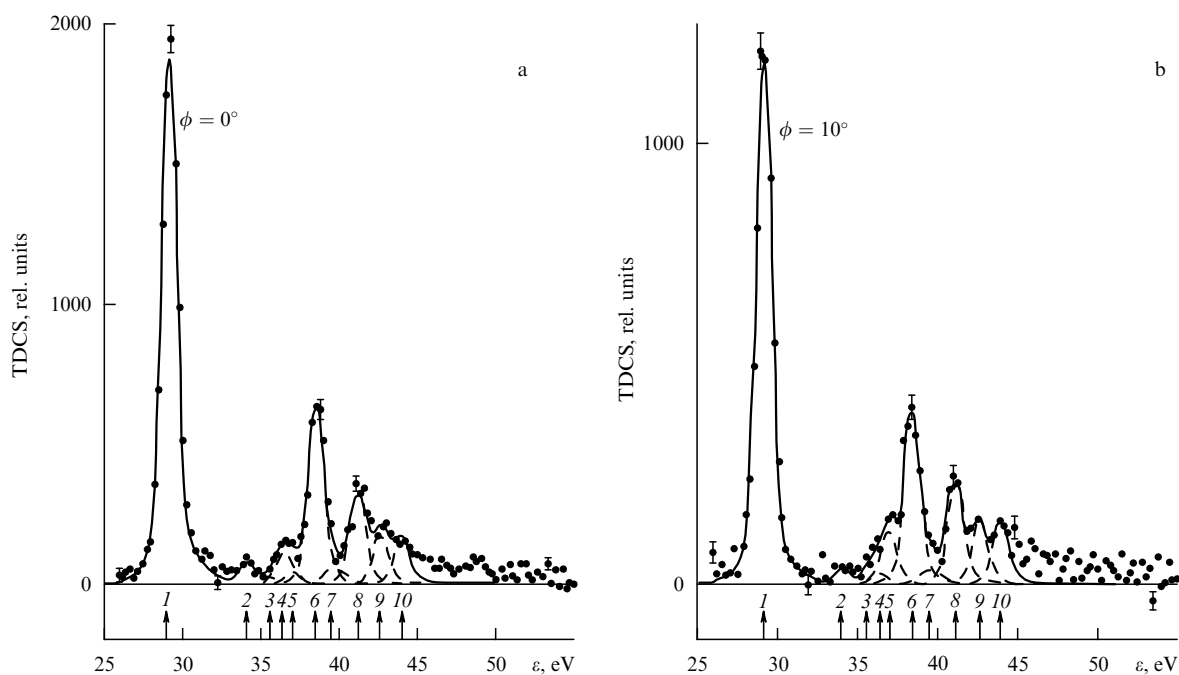


Figure 3. Energy spectrum of an argon atom measured in the symmetric kinematics of the EMS experiment for $\phi = 0^\circ$ (a) and 10° (b). Peaks 1, 4, 6, 8, and 9 belong to the 2S family; the rest of the peaks belong to families 2P and 2D ; $E_0 = 500$ eV [133].

energy spectrum structure and the form of angular differential cross sections. Helium represents a kind of test object for verifying various microscopic models in the scattering theory of several charged particles, including the models of the atomic wave functions with the direct inclusion of the ee-correlators (it is assumed that in a classical HF model the ee-interaction is taken into account implicitly, via the mean electric field).

The most abundant in nature is para helium, for which the coordinate part of the ground-state wave function is symmetric. It can be represented as the sum

$$\psi_i(\mathbf{r}_1, \mathbf{r}_2) = 4\pi \sum_{l=0}^{\infty} \Phi_{0l}(\mathbf{r}_1, \mathbf{r}_2) \langle Y_l(\mathbf{n}_1) | Y_l(\mathbf{n}_2) \rangle \quad (3.4)$$

over the angular correlations, where the function Φ_{0l} is calculated, as a rule, using the symmetrized products of the Laguerre type trial functions.

Taking into account expansion (3.4), after integration over dE_1 and the angular variables, expression (2.5) takes the form

$$\frac{d^3\sigma_n}{d\Omega_1 d\Omega_2 dE_2} = \frac{2^6 p_1 p_2}{\pi p_0} \left(\frac{d\sigma}{d\Omega} \right)_{ee}^{\text{Mott}} \sum_{l=0}^{n-1} (2l+1) \times \left| \int_0^{\infty} r_1^2 j_l(qr_1) dr_1 \int_0^{\infty} r_2^2 \varphi_{nl}(r_2) \Phi_{0l}(r_1, r_2) dr_2 \right|^2, \quad (3.5)$$

where $\varphi_{nl}(r)$ are the Coulomb functions of the stationary states in a field with the charge $Z = 2$, and $j_l(x)$ are the spherical Bessel functions. It is assumed in Eqn (3.5) that the hydrogen-like residual ion can be found both in the ground ($n = 1, l = 0$) and the excited state.

Helium constitutes a peculiar atom. Because of a large binding energy $\varepsilon_i = -79$ eV, the contribution Φ_{00} dominates with a weight of 94–98% in various simple and correlated models of the wave function ψ_i . It was found that almost all known models of the wave function yield the same cross section in the vicinity of a quasi-elastic peak. The EMS experiments cannot distinguish the details (Fig. 3a). To explain this fact, write out the expression for the momentum q in the case of the coplanar symmetric kinematics of the EMS experiment:

$$q \simeq \sqrt{2E_0} \left(1 - \frac{\cos\theta}{\cos\theta^*} \right), \quad \theta^* \simeq \frac{\pi}{4} - \frac{\varepsilon_{if}}{2E_0}. \quad (3.6)$$

It follows from Eqn (3.5) that for $n = 1$, the momentum $q = 0$ at the cross-section maximum. By expanding the integrand in Eqn (3.5) in a series in the vicinity of $q = 0$, we obtain

$$F_{ji}(\mathbf{q}) \simeq A - Bq^2. \quad (3.7)$$

Here, the term A determines the absolute value of the cross section, which has not been measured in earlier experiments and was substantially different (approximately by a factor of two) in the later experiments performed by different authors [85, 86], because they used different methods for evaluating the area of intersection of the electron and atomic beams. Thus, the term A in Eqn (3.7) cannot give definite information on the ground-state wave function.

In turn, the coefficient B determining the shape of a parabola is proportional to the integral

$$B \propto \int_0^{\infty} r_2^4 dr_2 \int_0^{\infty} r_1^2 \exp(-2r_1) \Phi_{00}(r_1, r_2) dr_1. \quad (3.8)$$

It follows from the latter expression that the integration over r_2 essentially ‘cuts’ the inner region of the helium one-particle wave function for $r_2 \leq |\varepsilon_i|^{-1/2} \simeq 0.5$ au, so that the coefficient B is substantially determined by its asymptotics, which should be the same of all ‘correct’ trial functions.

From the point of view of the study on ee-correlations, of most interest are the experiments in which the He^+ ion is excited to the state with the principal quantum number $n \geq 2$; we denote such reactions as $(e, 2e)^*$. In this case, the momentum distribution density has the form

$$\sum_f |F_{fi}(\mathbf{q})|^2 = \rho_n(q) = \sum_{l=0}^{n-1} (2l+1) \left| \int_0^{\infty} r_2^2 j_l(qr_2) dr_2 \int_0^{\infty} r_1^2 \varphi_{nl}(r_1) \Phi_{0l}(r_1, r_2) dr_1 \right|^2. \quad (3.9)$$

The term with $l = 0$ can no longer play the dominating role, and the contributions from the higher with respect to l waves should affect the cross section shape.

A series of symmetric experiments upon reactions $\text{He}(e, 2e)\text{He}_n^+$ with $n = 2$ and 3 was performed by Australian scientists in the mid-1980s [87]. The authors found that the experimental cross sections were substantially different from those calculated using the HF model. However, later on the correctness of the PWIA computations [87] was questioned [88], although the initial energy was 1.2 keV.

The use of distorted waves somewhat improved the situation and was substantiated by the fact that the excited state is spatially ‘broader’ than the ground state, and electrons spend ‘more time’ in the distorting atomic field.

In reality, the necessity of taking account of the distorted waves in experiments [87] stemmed from their noncoplanar geometry. If the momenta of the incident and knocked-out electrons do not lie in the same plane, the mechanism of quasi-elastic knock-out becomes not unique, and the internal multiple scattering should be taken into account. When the azimuthal angle is small, this can be easily performed by calculating eikonal corrections. In turn, the necessity of the noncoplanar kinematics of the experiments was caused by a substantial increase in the intensity of satellite spectral lines with increasing azimuthal angle.

Figure 4 illustrates the effect of explicit correlations on the shape of the differential cross section, when the residual ion resides in the ground state with the principal quantum number $n = 1$ and also when it is excited to the states with principal quantum numbers $n = 2$ and 3 [89]. The calculations were performed using the HF type wave function RHF of the helium atom from Ref. [80]:

$$\psi_i^{\text{RHF}}(\mathbf{r}_1, \mathbf{r}_2) = \Phi(\mathbf{r}_1) \Phi(\mathbf{r}_2), \quad \Phi(\mathbf{r}) = \sum_{i=1}^5 \alpha_i \varphi_i^{1s}(r), \quad (3.10)$$

and functions explicitly containing both radial and angular correlations, namely, one of the Silverman–Platas–Matsen (SPM) functions [90]

$$\psi_i^{\text{SPM}}(\mathbf{r}_1, \mathbf{r}_2) = \frac{1}{\sqrt{1+\lambda^2}} \left\{ N \left[\varphi^{1s}(r_1) \varphi^{1s}(r_2) + \varphi^{1s}(r_1) \varphi^{1s}(r_2) \right] + \frac{4\pi\lambda}{\sqrt{3}} \varphi^{2p}(r_1) \varphi^{2p}(r_2) \langle Y_1(\mathbf{n}_1) | Y_1(\mathbf{n}_2) \rangle \right\}, \quad (3.11)$$

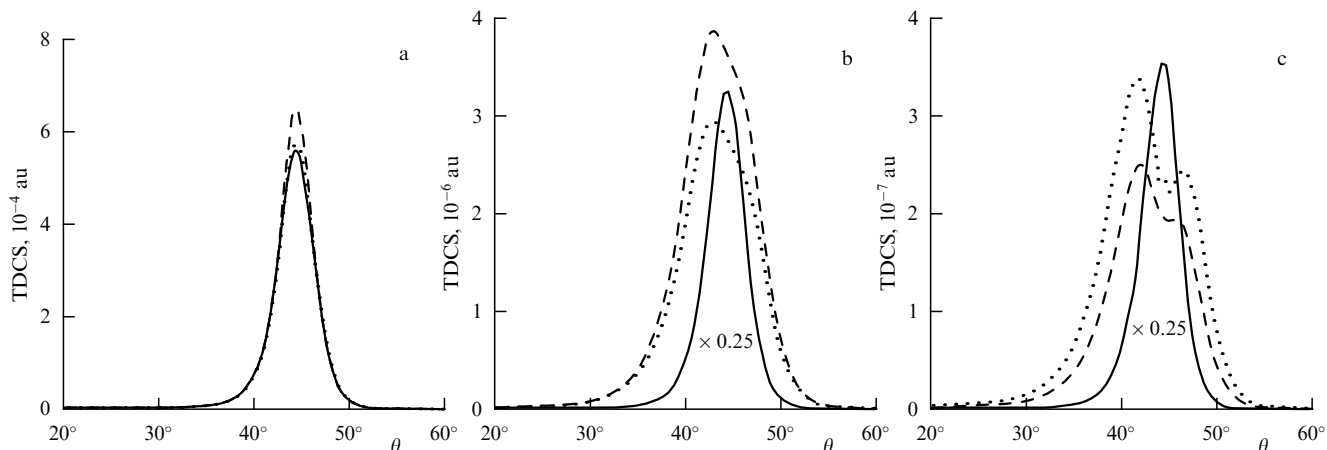


Figure 4. TDCS as a function of the scattering angle θ for the $\text{He}(e, 2e)\text{He}^+$ reaction: (a) $n = 1$; (b) $n = 2$, and (c) $n = 3$. The solid curve fits the RHF function (3.10); the dashed curve, the SPM function (3.11); the dotted curve, the H function (3.12); $E_1 = E_2 = 2$ keV [89].

and the Hilleraas (H) type function [91]

$$\psi_i^{\text{H}}(\mathbf{r}_1, \mathbf{r}_2) = N \left[\varphi^{1s}(r_1) \varphi^{1s'}(r_2) + \varphi^{1s'}(r_1) \varphi^{1s}(r_2) \right] (1 + C_0 e^{-\lambda r_{12}}). \quad (3.12)$$

In expressions (3.10)–(3.12), we set

$$\varphi^{1s}(r) = \sqrt{\frac{\gamma^3}{\pi}} \exp(-\gamma r), \quad \varphi^{2p}(r) = \sqrt{\frac{\delta^5}{3\pi}} r \exp(-\delta r),$$

where parameters γ and δ depend on the model type. Notice here that we denote the functions with explicit angular correlations by the spectroscopic symbol ($1s1s'$) (instead of $1s^2$) adopted in the modern scientific literature, which emphasizes that electrons occupy different s orbitals.

One can see that the cross sections for the models which take into account the ee-correlations explicitly differ in the absolute magnitude and shape from the cross sections for the HF wave functions with $n = 2$ and 3. It should be emphasized that the above-mentioned splitting of the quasi-elastic peak is mainly caused by radial ee-correlations, although expression (3.2) could suggest that this effect results from the admixture of the higher waves, i.e. from the angular ee-correlations. This conclusion follows from the almost complete coincidence of the cross sections calculated from Eqn (3.2) both by taking into account only the term with $l = 0$ and without this restriction, i.e. the p -waves do not play an important role in this case.

Let us try to explain an obvious discrepancy appearing in the description of an atomic target by different models (using different ‘languages’, as we wrote in Section 3.1). Consider in Eqn (3.9) only the term with $l = 0$. Let the function Φ_{00} be a symmetric sum of exponentials $\exp(\alpha_i r_1 + \alpha_j r_2)$ with some coefficients c_i . In that case, the double integral in Eqn (3.9) equals the sum

$$\sum_i \frac{c_i}{(q^2 + \alpha_i^2)^2}.$$

For $n = 2$, the inner overlap integral in formula (3.9) can become negative, which is impossible for $n = 1$. In addition to that if the exponents are different, the above sum can have several extrema and $q = 0$ will correspond to a minimum rather than to a maximum, which is just observed in the case

of the SPM and H wave functions. This is not the case for the RHF function, although it is also composed of a sum of exponentials.

From the physical point of view, this effect appears due to the conceptual difference in the structure of the 1S_0 states. Indeed, the use of the SPM and H wave functions with radial correlations allows one to consider two ionization mechanisms. In the first case, an electron is knocked out from the $1s$ state and the remaining electron passes from the $1s'$ state to the excited state of the He^+ ion because of the presence of the corresponding HF component in the expansion. In the second case, an electron is knocked out from the $1s'$ state, while the remaining electron passes from the $1s$ state to the excited state of the He^+ ion for the same reason. The interference in the amplitudes corresponding to these two mechanisms results in the shift of the binary peak to smaller angles, its smearing and even in its noticeable splitting into two peaks.

In the case of the HF function, both electrons are located in the same orbital, so that only the $(e, 2e)$ scattering is realized. In turn, the location of the electrons in different orbitals is explained by the fact that they are charged particles. One electron ‘sees’ a nuclear charge $Z = 2$ and is located closer to the nucleus by screening one charge unit, whereas another electron ‘sees’ a charge $Z = 1$ and is located farther from the nucleus. This qualitative picture corresponds to the now popular Temkin–Poet approximation (the s -atom) [92].

The trial HF type radial functions are usually written as a sum of products of the Laguerre polynomials and exponentials [80]. The expansion of the radial-correlated wave function of He in such a ‘Sturmian’ basis set results in a rather intense mixing of the (ns, ms) configurations, which is rarely employed in the HF calculations. According to the concept of the HF approximation, the explicit radial correlations are caused by intensive exchange processes. In this sense, the HF functions and Hilleraas functions are opposite to each other.

Thus, the above results show that the $(e, 2e)$ ionization of helium accompanied by the transition of the helium ion to the ground state gives us in fact no information on the type of the wave function of the helium atom (except a small decrease in the spectroscopic factor in the case of functions other than the HF functions). The boundedness of the angular range of measurements by the values $q \leq 2$ au does not allow one to make an unambiguous inference about the electron density at

small distances from the nucleus and about the short-range angular and even radial electron correlations. Hence there is a whole set of various trial wave functions that are physically equivalent for the description of MDs within the experimental error and considering the boundedness of the measurement range. This resembles somewhat the situation with the phase-equivalent potentials in nuclear physics.

At the same time, an atomic ionization accompanied by simultaneous excitation of the residual ion is more informative in this respect. First, such EMS experiments can be employed for studying radial ee-correlations, because their presence in a target substantially affects not only the absolute value but also the shape of the TDCS. In other words, the $(e, 2e)^*$ experiments give distinctive information about the type of the functions.

As for the angular ee-correlations, their presence in the wave function of a target only weakly affects the calculated cross sections. However, these conclusions are mainly result from the peculiarity of the He atom which is the most ‘compact’ atom, whereas in the case of heavier two-electron atoms, for example, Mg or molecules, both types of correlations should be considered.

In addition, taking into account expression (3.5), one can conclude that the EMS experiments with less ‘compact’ two-electron atomic targets, for example, negative ion H^- or an initially excited atom carry more information about the details of the wave function at distances more than 1 au from the nucleus. This is also valid for molecules (see Section 4).

3.3 Corrections to a plane wave impulse approximation

Helium can be conveniently used for studying the limits of applicability of the EMS technique based on the model of quasi-elastic impact and plane waves, because only few pure experiments have been performed with atoms in the EMS kinematics — either the initial energy of the beam was insufficient for expression (2.5) to be valid or the geometry of the experiment was noncoplanar. In the latter case, the quasi-elastic knock-out of the electron is no longer dominant and the contribution of the secondary processes should be accounted for.

Figure 5 shows results of a series of typical $(e, 2e)$ experiments with a helium atom for different initial energies E_0 [93]. One can clearly see that the PWIA and DWIA (Coulomb waves) calculations coincide in fact only for $E_0 \geq 3.6$ keV. For an energy 1.6 keV and higher, the shapes of the curves coincide but the absolute values are markedly different (note that the scale is logarithmic!). For $E_0 \leq 800$ eV, the difference between the PWIA and DWIA calculations and the experimental data becomes substantial. The experimental findings were normalized to the calculated results in the maximum of the differential cross section at $E_0 = 3.6$ keV.

Because complicated computations of the $(e, 2e)$ processes in molecules and solids are often performed in the PWIA, we will discuss below corrections to it introduced by other interaction mechanisms in order to find the limits of applicability of the model of quasi-elastic impact.

In Refs [81, 94] based on the theory of multichannel scattering of several particles, the expression

$$T_{fi}(\mathbf{p}_0; \mathbf{p}_1, \mathbf{p}_2) = Z^{1/2} \int \frac{d\mathbf{p}'_1 d\mathbf{p}'_2 d\mathbf{q}'}{(2\pi)^3 (2\pi)^3 (2\pi)^3} \langle \psi_f^- (\mathbf{p}_1, \mathbf{p}_2) | \mathbf{p}'_1, \mathbf{p}'_2 \rangle \times \langle \chi_1^- (\mathbf{p}'_1), \chi_2^- (\mathbf{p}'_2) | \hat{t}_{ee}(E - \varepsilon_f) | \chi_0^+ (\mathbf{p}_0), \mathbf{q}' \rangle F_{fi}(\mathbf{q}') \quad (3.13)$$

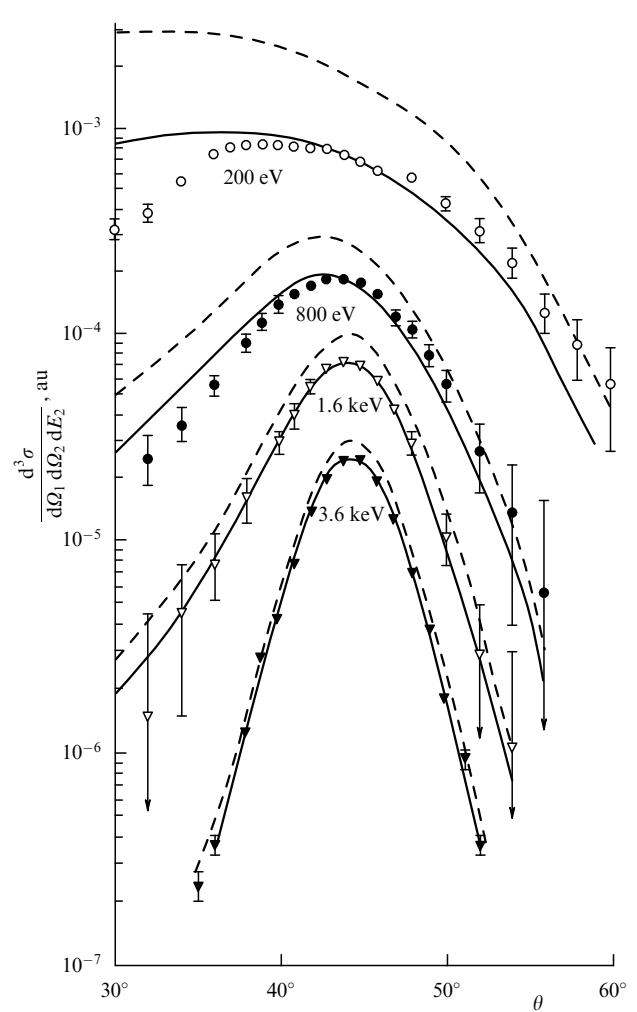


Figure 5. TDCS as a function of the scattering angle θ for the $He(e, 2e)He^+$ reaction at different initial energies E_0 . The solid and dashed curves were calculated in the DWIA and PWIA, respectively [79].

was obtained for the matrix element of a single $(e, 2e)$ collision with an outer-shell electron, which supplements formula (2.3). The one-particle wave functions $|\chi_i^\pm(\mathbf{p})\rangle$ in Eqn (3.13) correspond to the outgoing or ingoing wave distorted by the mean atomic field. The potential of this field in a complex target is usually represented by a square well potential, which in turn leads to the representation of the distorted wave in the form of a plane wave directed along the vector \mathbf{p} , with the wave number found from the expression $p = [2(E + \bar{V})]^{1/2}$. The potential \bar{V} of the mean atomic field includes both the real and imaginary parts. In a particular case of a high-energy particle or a weak field, we obtain eikonal corrections distorting the phase of the plane wave.

However, because electrons are the charged particles, the theory of scattering by short-range potentials cannot be formally applied to the $(e, 2e)$ scattering [95, 96]. In Refs [81, 94], quantitative corrections to the PWIA results, caused by the interaction of electrons at the atom periphery and related to the term $\langle \psi_f^- (\mathbf{p}_1, \mathbf{p}_2) | \mathbf{p}'_1, \mathbf{p}'_2 \rangle$ in expression (3.13), were found. Their physical background is quite simple: during their motion from ‘the atomic surface’ which can be, for example, the outer electron shell to the detectors, the electrons will continue attracting the ion ($Z = 1$) and repulsing from each other. As a result of this peripheral process, the electron paths bend and they enter the detectors at larger angles

compared to those in the case of straight-line motion. Therefore, the experimental curve of the differential cross section shifts to larger angles compared to the PWIA calculations. The same conclusions were drawn by Gailitis [97].

By neglecting the peripheral Coulomb interaction, we obtain

$$\langle \psi_f^-(\mathbf{p}_1, \mathbf{p}_2) | \mathbf{p}'_1, \mathbf{p}'_2 \rangle = (2\pi)^6 \delta(\mathbf{p}_1 - \mathbf{p}'_1) \delta(\mathbf{p}_2 - \mathbf{p}'_2) \quad (3.14)$$

and arrive at the DWIA expression (3.13). The idea of using the optical potential for calculations of the distorted waves was successfully developed in the 70s–80s by McCarthy, Weigold et al. [98]. The advantage of their model is that it simplifies expression (3.10) and eliminates the integration over \mathbf{q}' , because the amplitude $\langle \mathbf{p}'_1, \mathbf{p}'_2 | \hat{t}_{ee}(E - \varepsilon_f) | \mathbf{p}_0, \mathbf{q}' \rangle$ includes the law of conservation of momentum $\delta(\mathbf{p}'_1 + \mathbf{p}'_2 - \mathbf{p}_0 - \mathbf{q}')$. This circumstance again leads to the factorization of the amplitude into the structural and dynamic cofactors.

With advances in computer technology the above analytic model was replaced by more developed models of the distorted waves and computational algorithms borrowed from nuclear physics. However, the ‘optical’ eikonal which has a clear physical meaning proved to be useful for the qualitative explanation of relativistic (e, 2e) experiments [82] performed with inner atomic shells of Cu and Ag, as was mentioned above. Notice that the DWIA calculations also result in the shift of a curve of the differential cross section to larger angles, thus improving the agreement with the experiment.

Thus, the theory of the (e, 2e) ionization contains (along with corrections related to the distortion of the electron plane waves by a central mean field and inherent in any scattering theory) three-particle distortions, which are specific for Coulomb scattering and are caused by the long-range interaction. Their effect can be conveniently estimated using the semiclassical approximation of quantum mechanics [99] [in fact, the delta functions in Eqn (3.14), reflecting the straight-line motion of the ejected electrons, should be replaced by delta functions along their classical paths]. For this reason, we shall call such corrections the three-particle semiclassical corrections as opposed to the eikonal corrections which are related only to the two-particle dynamics of a free electron motion in a mean atomic field (although both these corrections are actually semiclassical).

The eikonal phase corrections to the plane waves in functions $|\chi_f^\pm(\mathbf{p})\rangle$ can make a much greater asymptotic contribution to the differential cross section, because they are proportional to $E_0^{-1/2}$ (see, for example, Ref. [66], Ch. C5), whereas semiclassical corrections for the path bending are proportional to E_0^{-1} [81]. The eikonal corrections remained in the high-energy asymptotics, so that the DWIA represents a natural ‘analytic’ continuation of the PWIA. However, the semiclassical corrections which have no analogs in the conventional scattering theory also play an important role in practice.

Figure 6 displays the ratio of the experimental and theoretical cross sections for the He(e, 2e)He⁺ ionization in the EMS geometry in a broad range of the initial energies, taking into account only semiclassical corrections [81]. One can see that the deviation of the theory from the experiment does not exceed 20% even for comparatively low energies. It seems likely that calculations for medium energies should

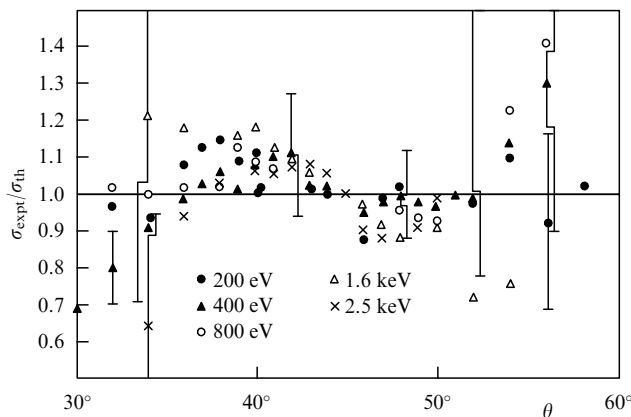


Figure 6. Ratio of experimental cross sections to the theoretical ones calculated taking into account only semiclassical corrections for different initial energies E_0 [81].

consider both eikonal and specific semiclassical corrections; however, such combined calculations have not been performed so far.

Let us estimate the range of applicability of the PWIA model. It follows from the virial theorem that the mean field potential $\bar{V} \simeq 2\varepsilon_0$, where ε_0 is the energy of the ionized shell. In this case, the condition of smallness of eikonal corrections has the form

$$\frac{\bar{V}r_0}{p_{a(b)}} \ll 1 \quad \text{or} \quad \frac{2\varepsilon_0 r_0}{\sqrt{E_0}} \ll 1, \quad (3.15)$$

where r_0 is the radius of the ionized electron shell. Because $\varepsilon_0 r_0^2 \sim 1/2C^2$, where C is a constant of the order of unity, criterion (3.15) takes the form

$$C\sqrt{\frac{2\varepsilon_0}{E_0}} \ll 1.$$

The PWIA and DWIA calculations give close results for most atoms at $E_0 \simeq 3$ keV [96].

4. Electron orbitals in molecules

It was noted in Section 1 that general information on the shape and size of molecules can be obtained, for example, from elastic scattering of high-energy electrons. The (e, 2e) technique has another advantage. It allows one to directly ‘see’ an individual molecular orbital (MO) in the momentum space, its structure as a linear combination of atomic orbitals (LCAO), and to distinguish bonding and antibonding orbitals. In addition, this technique permits one to study the ee-correlations, which can strongly affect the inner valence orbitals, and the deformation of the outer occupied MOs upon the complex formation, being a first step in the ‘microscopic’ study on the reactivity of molecules, etc.

We showed in Section 3 how different MDs for s and p electrons in atoms are (the MD for d electrons at small q is proportional to q^4 rather than to q^2 , as for p orbitals, which can be distinctly revealed in experiment). This results in the high sensitivity of the (e, 2e) technique to the sp -hybridization of individual bonding orbitals (in particular, the $3\sigma_g$ orbital of the N_2 molecule) [7]. For example, the degree of sp -hybridization producing directed C–H bonds in the CH_4 molecule presents an important parameter of the MO LCAO approxi-

mation. The hydrogen $1s$ orbital differs from the carbon $2s$ orbital by the width of the MD, and their contributions can be determined from the shape of a peak located at $q = 0$. The detailed analysis of contributions of the LCAO terms to the measured electron MDs for the outer occupied orbital in acetone $(\text{CH}_3)_2\text{CO}$ ($2p$ electrons of oxygen, the C–H σ -bond of methyl groups CH_3 , etc.) was performed in paper [100].

It is important to note that the $(e, 2e)$ technique reliably distinguishes bonding and antibonding MOs constructed from the same atomic components [7, 14]. This is possible due to the interference in the amplitudes of the electron knock-out from the orbitals belonging to different centers. Its role is clearly revealed when the spatial structure of a molecule is known (see Section 2.2). For example, the σ_g orbital of the homonuclear N_2 molecule is represented by the sum of atomic orbitals $2s_a + 2s_b$. The interference in the waves from centers a and b upon the electron knock-out results in the appearance of the multiplier $1 + (\sin qR)/qR$ in the amplitude, which is approximately equal to 2 for small q . In this case, the MD qualitatively retains the s shape of the atomic orbital. The analogous molecular σ_u orbital is represented by the difference of atomic orbitals $2s_a - 2s_b$ and contributes the destructive interference multiplier $1 - (\sin qR)/qR$ to the amplitude. As a result, the MD acquires the p shape because the above multiplier becomes zero for $q \rightarrow 0$. For this reason, the hybridization from atomic s and p orbitals in the nitrogen molecule is distinctly observed for bonding $3\sigma_g$ orbitals and is poorly revealed in antibonding $3\sigma_u$ orbitals [7, 14, 101].

This is illustrated by the MD for the $3\sigma_g$ orbital in the F_2 molecule [101], presented in Fig. 7, where both s and p components of the hybridized orbital are distinctly identi-

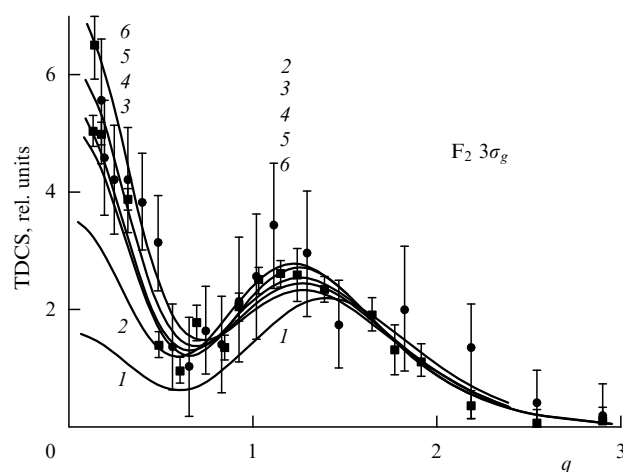


Figure 7. TDCSs for the $3\sigma_g$ orbital of the F_2 molecule. Curves 1 and 2 correspond to the HF models of the orbital; curves 3–5, to the CIA models (their specification is insignificant for our purposes); $E_0 = 1.5$ keV [101].

fied. At the same time, the ee -correlations should be taken into account for the consistent quantitative description (see below).

As a more scaled example of the use of the above concepts, consider in the framework of the $(e, 2e)$ method the widely discussed question of how donor–acceptor bonds are changed in hydrogen-containing inorganic molecules such as H_2O , NH_3 , PH_3 upon the successive replacement of hydrogen atoms by methyl groups CH_3 . Figure 8 presents the electron MDs for the highest occupied molecular orbital

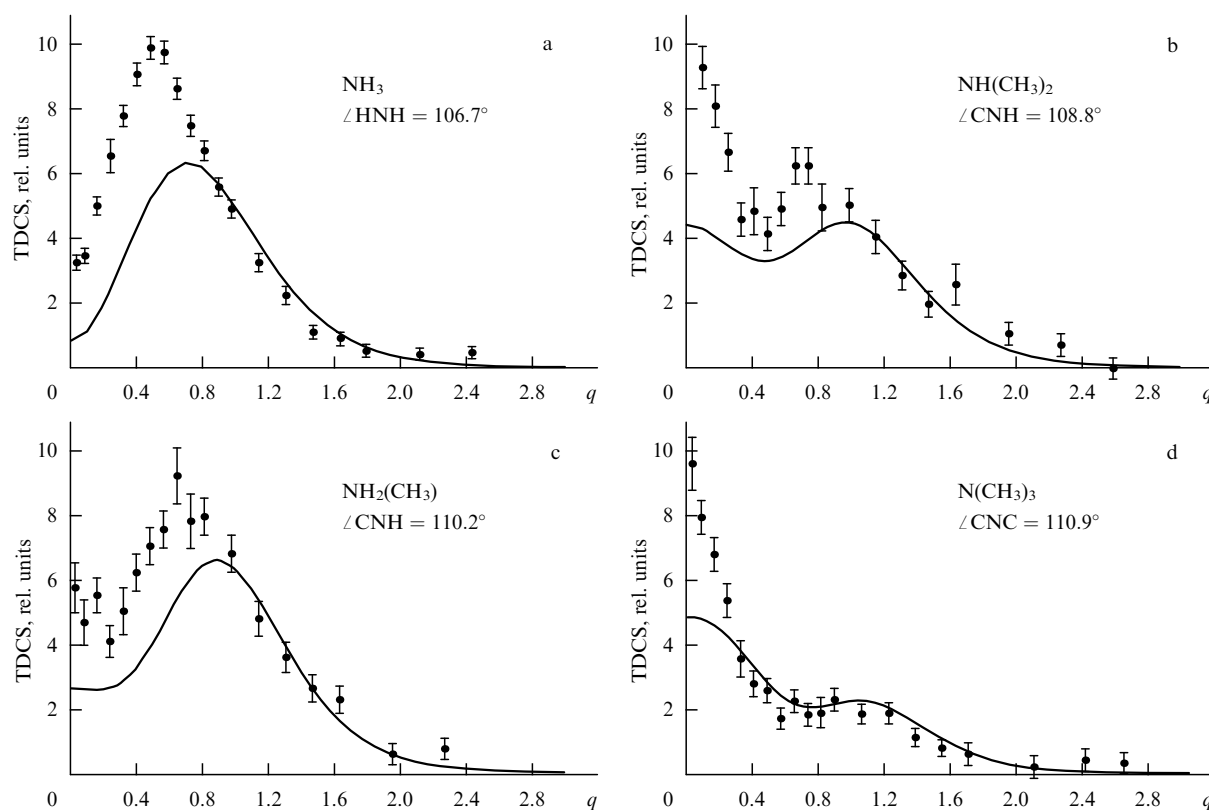


Figure 8. Spherically symmetric TDCSs for the outer valence orbitals of molecules NH_3 , $\text{NH}_2(\text{CH}_3)$, $\text{NH}(\text{CH}_3)_2$, and $\text{N}(\text{CH}_3)_3$; $E_1 = E_2 = 600$ eV (see details of calculations in Ref. [102]).

(HOMO) in molecules NH_3 , $\text{NH}_2(\text{CH}_3)$, $\text{NH}(\text{CH}_3)_2$, and $\text{N}(\text{CH}_3)_3$ [102]. One can see that the MD with a small contribution of the s orbital, which is close to the p shape and typical of the NH_3 molecule, is rapidly displaced by the MD with a larger contribution of the s orbital inherent in the CH_3 group.

If the NH_3 molecule is characterized by a partial displacement of the electron density from H atoms to a central N atom, then the replacement of H atoms by methyl groups CH_3 is accompanied by the reverse redistribution of the electron density from the N atom to methyl groups CH_3 . In accordance with the increasing weight of the s -component, the angles between bonds increase from 106.7° for the NH_3 molecule to 110.9° for the $\text{N}(\text{CH}_3)_3$ molecule (see analogous comparison of molecules H_2O , H_2S , H_2Se , and H_2Te in Ref. [101]).

Similar behavior was observed for a series of molecules PH_3 , $\text{PH}_2(\text{CH}_3)$, $\text{PH}(\text{CH}_3)_2$, and $\text{P}(\text{CH}_3)_3$ [103] as well as H_2O , $\text{H}(\text{CH}_3)\text{O}$, and $(\text{CH}_3)_2\text{O}$ [104]. As a whole, this effect is well described in the framework of the HF approximation providing the basis of the MO LCAO method.

At the same time, there are a number of examples pointing to a very high sensitivity of the $(e, 2e)$ process to the ee -correlations in the target. This is manifested in the appearance of satellites of the basic transitions, resulting in a decrease in the intensity of the latter, as well as in the shape of the MDs characterizing these transitions. Figure 9 demonstrates the most often cited example of this kind — the MD for the outer occupied $1b_1$ orbital of the H_2O molecule, where the $2p$ orbital of the O atom is the main component of the LCAO [34, 105] (the deviation of the theory from the experiment for small q is explained by the finite angular resolving power of counters). One can see that both the wave functions of the molecule and the ion, calculated in the configuration interaction approximation (CIA), quantitatively describe the experiment. Notice here that the CIA gives for this orbital a value of the spectroscopic factor $S_{00} = 0.86$, i.e. only 14% of the intensity is transferred to the correlation satellites (see below the case of the I_2 molecule). Figure 9 shows that the

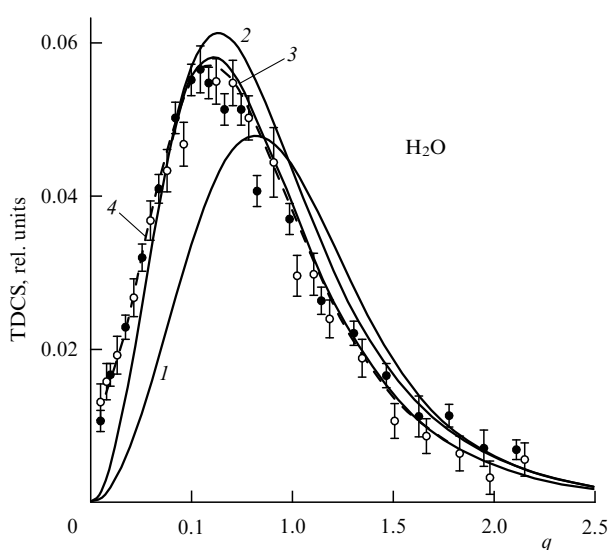


Figure 9. TDCSs for the outer filled $1b_1$ orbital of the H_2O molecule. Curves 1 and 2 correspond to the HF models of the orbital; curves 3 and 4 include the configuration interaction (see details of calculations in Ref. [34]).

$(e, 2e)$ technique is capable of distinguishing rather fine effects related to the ee -correlations in molecules.

Notice that it is the CIA wave function (which quantitatively complies with the experiment) that gives simultaneously the experimental dipole moment of the H_2O molecule and the binding energy of a water dimer, thereby describing adequately the van der Waals forces [34]. This is a typical feature of modern studies (see analogous extended description of the data collection in Ref. [32], where the MDs for the valence orbitals in the NO molecule were presented).

The next example is related to the extensively studied series of diatomic homonuclear halogen molecules. We noted in the discussion of Fig. 7 that the HF approximation cannot describe quantitatively the MD for the $3\sigma_g$ orbital of the F_2 molecule (because the ee -correlations in a target should be taken into account). The relevant CIA calculations [100] shown by curves 3–5 in the same figure quantitatively comply with the experiment.

The density functional theory (DFT) [106] also well describes the experiment (curve 6 in Fig. 7). This theory was put forth in the known paper by Kohn and Sham [107], where the one-particle Schrödinger equation was solved with a nonlocal potential taking into account the ee -correlations and some exchange effects. Examples with the F_2 molecule and other simple molecules bring out that the DFT which significantly simplifies numerical calculations (in contrast to the many-particle CIA) adequately reflects correlation effects and can be very useful in the description of complex molecules. However, the DFT, like any other one-particle potential approach, cannot be used for calculating the spectroscopic factor of an electron.

The spectroscopic factor S_f introduced by Eqn (2.8) is an important parameter of the many-electron wave function of a molecule. First of all, this factor indicates the branching character of its couplings with the states of a final molecular ion, which is manifested in the breakdown of the main transition peak in the energy $(e, 2e)$ spectrum into a family of satellites, whose relative intensities reflect the degree of excitation of the different hole states (see Fig. 3 and Ref. [22]). It was found from measurements of the MDs and spectroscopic factors that the correlation effects are comparatively weak for the highest occupied (i.e. outer) orbitals of halogen molecules [108]. However, when passing from the light molecules (of the F_2 type) to heavy ones (of the Br_2 and I_2 types), excitation of the correlation satellites accompanied by ionization of the inner valence orbitals dramatically increases, and the basic transition in the I_2 molecule (which would be the only one in the HF approximation) becomes weaker upon the electron knock-out from the $10\sigma_g$ or $10\sigma_u$ orbital. The intensity of this transition is imparted to the satellites, resulting in its 'sinking' in them and smearing over a broad energy interval of many-particle excitations. The basic-transition intensity also depends on the relaxation effect, i.e. on the variation in the self-consistent field caused by the hole appearance [109]. An important role of the correlation satellites manifested through the decrease in the spectroscopic factor was also found for hydrogen halides [110].

When passing to complex molecules, the ee -correlations more strongly affect the shape of the MD of electrons in valence orbitals, compared to the changes shown in Figs 7 and 9. Figure 10 presents the MD for the $1e''$ orbital of the [1, 1, 1]-molecule of propellane C_5H_6 [111]. One can see that the model which takes into account the ee -correlations (curve 1) and is in good agreement with the experiment, effects the MD

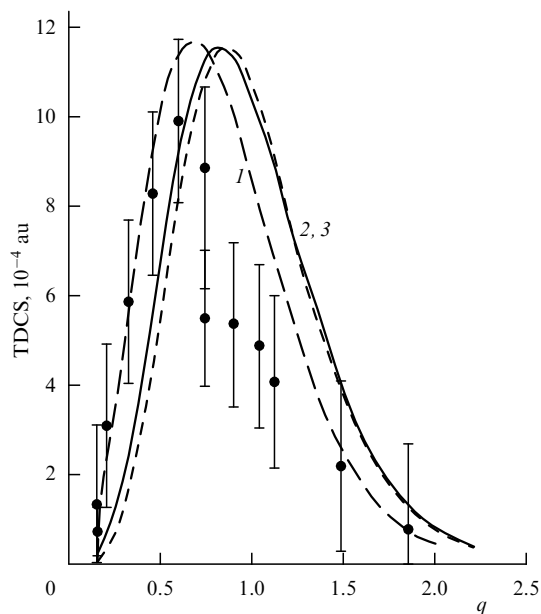


Figure 10. TDCSs for the $1e''$ orbital of the [1, 1, 1]-molecule of propellane C_5H_6 . Curve 1 includes the configuration interaction; curves 2 and 3 do not include this interaction; $E_0 = 1$ keV (see details of calculations in Ref. [114]).

shift to the left (to lower momenta q) compared to variants of the self-consistent field approximation, i.e. because of the ee-repulsion, the electron cloud shifts to the periphery of a molecule, in contrast to the HF approximation. The result is enhanced with increasing the size of the molecule and the number of valence electrons in the system.

The improved sensitivity to the ee-correlations in conjunction with the fact that the CIA calculations of more complex molecules become too cumbersome resulted, despite the above-mentioned drawbacks, in the wide application of the DFT for analysis of the (e, 2e) MDs of electrons occupying valence orbitals of complex molecules [112]. Bearing in mind more general aspects of these problems it is worth mentioning that the most important problem of molecular quantum theory and quantum chemistry is a microscopic electron theory of molecular reactivity (chemical reactivity), which requires first of all the (e, 2e) data on the structure of outer molecular orbitals [106] and (which is especially complicated) on their variation when two colliding

molecules approach each other. However, just these data are within the grasp of the present-day experimentation.

Figure 11 shows the electron MD for the $11f_1$ orbital of the $(CH_3)_3N-BF_3$ complex [112]. Compared to its molecular components, the complex is a very loose system which can be treated as a model of chemically interacting molecules. One can also see from Fig. 11 that the $6a_1$ orbital of trimethylamine is substantially transformed in passing to the complex, namely, the type of its sp -hybridization (i.e. the shape of the directed electron clouds) changes. The quantitative analysis of the data presented in Fig. 11 showed that a certain displacement of the electron cloud from nitrogen to boron takes place [112].

A similar conclusion was drawn in paper [36] where the substantial effect of the mutual arrangement of parts (viz. conformation) of the dimetoxymethane $(CH_3O)_2CH_2$ molecule (of interest for biology) on the MDs of outer-orbital electrons was found by means of the DFT and (more indirectly) experimentally. With this striking demonstration of plasticity it was natural to conclude that HOMO, being so highly deformable, which is manifested in the redistribution of electrons between orbitals of different atoms, are mainly responsible for the chemical reactivity [112]. This is a very promising field of investigation.

So far it has been assumed that a residual ion retains the geometry of a molecular target. A change in the molecular spatial structure caused by electron knock-out [113, 114] can complicate the interpretation of the MD but, fortunately, rarely plays an important role. It was noted in Ref. [113] that if the electron is knocked out from the γ orbital with the wave function ψ_γ which is not symmetric (i.e. not invariant upon molecular symmetry-group transformations) and the symmetry of the final-ion equilibrium configuration differs from the symmetry of the initial molecule, then the MD is no longer zero for $q = 0$.

Let us denote the equilibrium nuclear coordinates in the initial molecule and in the final molecular ion by Q_0 and Q'_0 , respectively, and the average value of these quantities by \bar{Q} . The value of \bar{Q} depends on the vibrational state being excited [114]. The molecular symmetry for the nuclear configuration \bar{Q} is lower than that for the Q_0 configuration. In this case, we have

$$\psi_\gamma(\mathbf{q}, \bar{Q}) = \alpha\psi_\gamma(\mathbf{q}, Q_0) + \beta\psi_{a_1}(\mathbf{q}, Q_0) + \dots, \quad (4.1)$$

where a_1 is a symmetric orbital with the s -shape MD; for this reason, $|\psi_\gamma(\mathbf{q} = 0, \bar{Q})|^2 \neq 0$ due to the second term in the

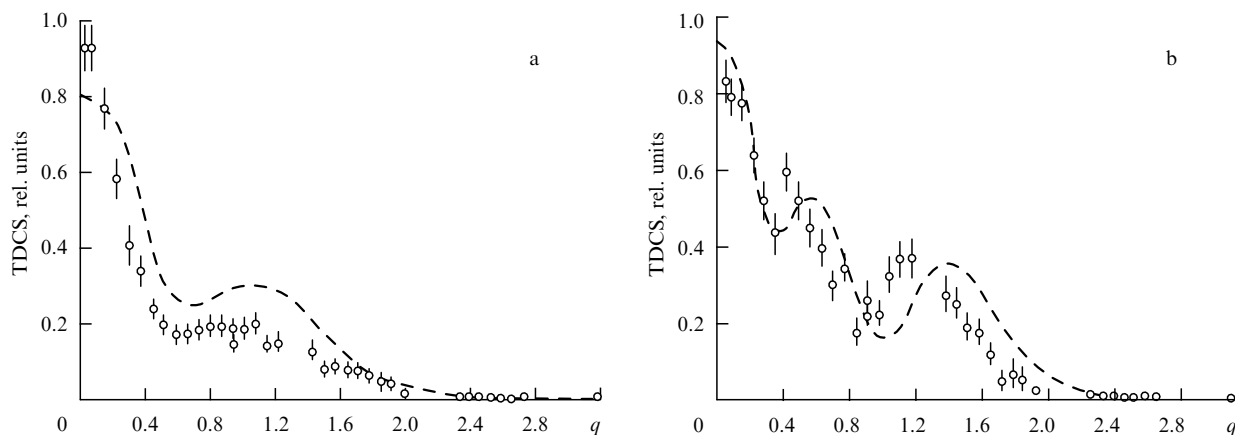


Figure 11. TDCSs for (a) the $6a_1$ orbital of the $N(CH_3)_3$ molecule, and (b) the $11f_1$ orbital of the $(CH_3)_3N-BF_3$ complex [112].

expansion. The property of a ‘partial filling of zero’ appears upon electron knock-out from orbitals that do not possess total symmetry both for nondegenerate and degenerate states of the final molecular ion.

Indeed, the geometry of the degenerate states of the final molecular ion changes due to the Jahn–Teller effect [113, 115] which results in splitting of the energy levels γ_a emerged in the (e, 2e) spectrum. The wave function of each of the levels

$$\psi_{\gamma a}(\mathbf{q}, \bar{Q}) = \sum_i C_{ia}^{\gamma}(\bar{Q}) \psi_{\gamma i}(\mathbf{q}, Q_0) \quad (4.2)$$

reflects mixing of the initial degenerate states $\psi_{\gamma i}(\mathbf{q}, Q_0)$ between themselves, caused by the symmetry lowering. Because the expression for the scattering cross section contains the MD averaged over molecular orientations (see Section 2), we are dealing finally with the quantities

$$\int d\Omega_q |\psi_{\gamma a}(\mathbf{q}, \bar{Q})|^2 = \sum_i |C_{ia}^{\gamma}(\bar{Q})|^2 \int d\Omega_q |\psi_{\gamma i}(\mathbf{q}, Q_0)|^2. \quad (4.3)$$

The second integral in the last formula is independent of the degeneration index i , similarly to the independence of the atomic form factor from the total magnetic quantum number in the general case. For this reason, because the system of functions $\psi_{\gamma i}$ is orthonormal, the equality $\sum_i |C_{ia}^{\gamma}(\bar{Q})|^2 = 1$ is valid. That is the first integral is independent of the subscript a . This means that the MD is the same for each γ_a orbital.

Thus, both the vibrational broadening of the hole level and the broadening caused by the Jahn–Teller effect are manifested in the interesting property: $|\psi_{\gamma}(\mathbf{q} = 0, \bar{Q})|^2 \neq 0$, despite the fact that the electron is knocked out from the degenerate orbital [113, 114]. The larger the distinction between configurations Q_0 and Q'_0 , the greater the difference of the MD from zero for $q = 0$. Figure 12 illustrates the urgency of this problem. Here, the MD is shown for the outer degenerate $3e'$ orbital of cyclopropane C_3H_6 molecule having D_{3h} symmetry [113]. The ion symmetry is lowered to C_{2v} due

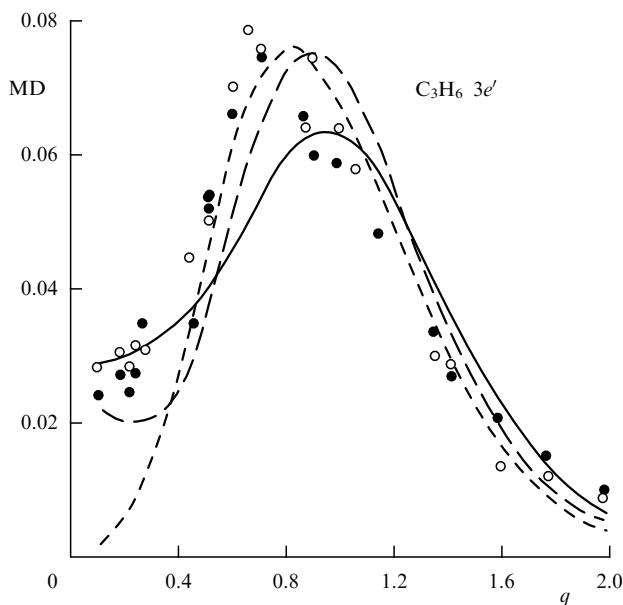


Figure 12. MDs for the $3e'$ orbital of the cyclopropane C_3H_6 molecule. The light and dark circles are experimental data for the first (less coupled) Jahn–Teller component and the second component, respectively (see details of calculations in Ref. [113]).

to the Jahn–Teller effect, and the ground state of the ion is split into two energy-discriminated components which can be experimentally resolved. One can see that, firstly, the $D_{3h} \rightarrow C_{2v}$ lowering of the symmetry results in a noticeable filling of the MD zero (i.e. $\beta \neq 0$ in formula (4.1)) and, secondly, the MDs of both components are identical.

5. Electron orbitals in crystalline and amorphous solids

The EMS of solid targets substantially differs from that of atoms and molecules by the experimental procedure. There are two types of (e, 2e) experiments: with ‘shooting’ through a self-supporting film of thickness about 100 Å, and with ‘reflection’ from the sample surface. Because most of the experiments with solid targets have been performed in the shooting mode, we will discuss them in this section.

The study of the (e, 2e) process in a solid is characterized by the stepwise overcoming of severe methodical problems. Thus, to reduce the multiple scattering of electrons in a sample to a reasonable level, high-energy electrons are required (of order 20 keV and above). However, the cross section of free (e, e) scattering accompanied by the transfer of a sufficiently large energy (several keV) to the knocked-on electron is small. Below, we consider the results of studies performed by the group of I McCarthy and E Weigold (Australia) with the initial electron energy $E_0 = 20$ keV and energies of knocked-out electrons $E_1 = 18.8$ keV and $E_2 = 1.2$ keV. In the case of such asymmetric kinematics, the scattering cross section is not very small, but because of the small value of E_2 only a thin layer of thickness 30 Å at the rear surface of a film is actually studied. Here, we encounter another difficulty, namely, an important role, under certain conditions (even for very thin films), of multiple elastic and inelastic electron scattering accompanied by creation of plasmons. Fortunately, the multiple scattering of electrons with energies 1 keV and above is well simulated by the Monte Carlo method [116], and such a background is taken into account in the analysis of the experiment. To exclude the effect of multiple scattering, Weigold and coworkers are making the experimental complex with energies $E_0 = 50$ keV and $E_1 = E_2 = 25$ keV [19] by retaining the energy resolution $\Delta E \leq 1$ eV and the momentum resolution $\Delta q \simeq 0.1$ au achieved to date.

The first subject that we will consider here concerns an Al polycrystal and its valence band, which furnish an example of how the electron Fermi gas ‘appears’ in a metal in studies by the (e, 2e) technique. Figure 13 compares the MDs (i.e. spectral densities for different binding energies ε of the knocked-on electron in the conduction band [25, 26, 44, 118]) with the theoretical result [117] obtained in the well-known muffin-tin (MT) potential approximation (see, for example, Ref. [119]). This approximation corresponds to a choice of electron wave function in the conduction band in the form of a plane wave, which means the complete conformity of the electron momentum \mathbf{q} to the quasi-momentum \mathbf{k} . In addition, in calculations the form factor was convoluted with a Gaussian distribution modelling the finite experimental energy resolution. One can see from Fig. 13 that a single peak typical for each value of ε upon varying the quasi-momentum k does not reveal any appreciable ‘inner’ width, i.e. the parabolic law of dispersion $\varepsilon(\mathbf{k}) = \varepsilon_0 - k^2/2m^*$, where $m^* = m_e = 1$, is confirmed. In this case, the role of multiple scattering near the Fermi surface ($\varepsilon = 4$ eV) is negligible.

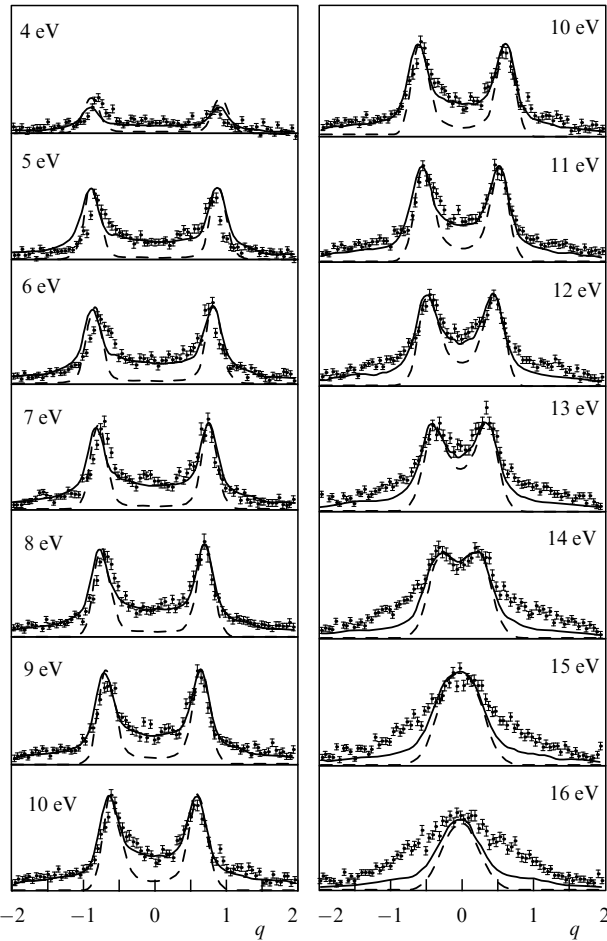


Figure 13. Series of MDs for polycrystalline Al for different binding energies ε within the valence band. The solid curves are calculated taking into account multiple scattering for the MT potential by the Monte Carlo method; the dashed curves are calculated by neglecting multiple scattering [117].

Thus, the example considered in Fig. 13 corresponds to the well-known physics of a Fermi gas and demonstrates the methodical reliability of the (e, 2e) technique. Note in addition that this figure also shows how an increase in the binding energy of the knocked-on electron (an approach to the band bottom, $\varepsilon = 16$ eV) results in a significant enhancement of negatively manifested multiple scattering. This hinders at present the study of a number of interesting effects (the plasmaron satellite in the conduction band and the Mahan–Nozieres effect discussed in Section 2.3) typical for the states below the bottom of the conduction band. New experimental complex that is now in the making in Australia will permit the investigation of such effects to be launched.

The second, more physically complicated example is related to the study on the valence band of a graphite single crystal. It is known that graphite has a scaly structure and its (x, y) plane contains the σ band characterized by the sp^2 configuration of the carbon atom. The corresponding hybridization from the s and p orbitals leads to hexagonal flat cells in graphite. For this reason, the dispersion curve for the σ band is anisotropic. This is clearly seen from Fig. 14, where the results of the (e, 2e) experiment [40] show that this curve differs by appearances in the ΓK and ΓM directions. Theoretical calculations took into account the experimental resolutions ΔE and Δq but neglected multiple scattering [40].

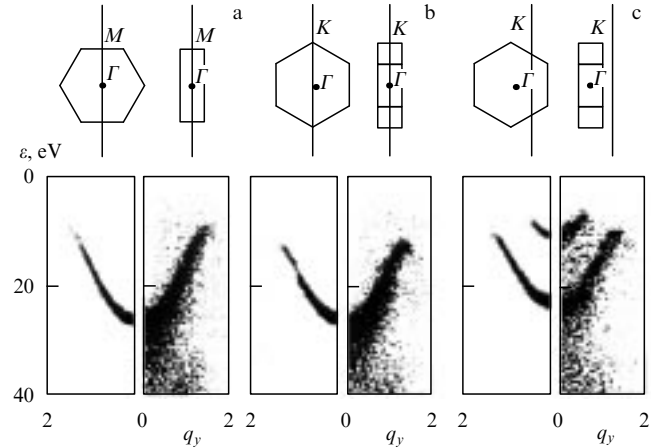


Figure 14. MD as a function of the binding energy and momentum q_y (the maximum intensity reflects the law of dispersion) for three different measurement geometries (see the text). In the left halves of the figures, the calculated results in the MT approximation with the resolutions $\Delta E = 2$ eV and $\Delta q = 0.1$ au are presented [40].

The anisotropy (i.e. the sensitivity to special features of a lattice) is observed only in the upper part of the dispersion curve. In the ΓM direction, this curve encloses σ_1 and σ_2 bands with the boundary between them at $q = 0.8$ au and the gap of about 0.5 eV (which is not observed in the (e, 2e) experiment), while in the ΓK direction the dispersion curve emerges from the σ_1 band to the σ_3 band.

A graphite single crystal well illustrates an important property of the (e, 2e) technique, namely, the possibility of choosing the real electron momentum \mathbf{q} in the crystal in any specified direction (this is directly performed by choosing the angles Ω_1 and Ω_2 of counters and energies E_1 and E_2 [19]), viz. to move through the band by changing \mathbf{q} in a rigidly controllable way.

In the z direction, where the distance between atoms is greater than that in the (x, y) plane, the π band is formed with the lower electron binding energies. In contrast to the σ band, the minimum of energy of the π band corresponds to a quite large momentum q_z . The difference between the σ and π bands is explained as follows [120] (we present this explanation here because it is closely related to the type of electron MD in the band).

The bonding σ orbital in a crystal consists predominantly of symmetric sums of the atomic $2s$ orbitals (similarly to the σ_g orbital of diatomic molecules; see Section 4). A state of valence electrons in the σ band with the maximum charge density between nuclei in all crystal cells proves to be the most energetically favorable. The wave function of this state has a large constant component in the coordinate representation.

From the point of view of the Fourier transform to the momentum representation, this means that the electrons near the bottom of the band have almost zero momentum; in other words, the form factor $|F_\sigma(q)|^2$ reaches a maximum for $q = 0$ (near the band bottom). In turn, the $2p$ electrons which also take part in the formation of the σ band make no contribution to the maximum of the MD at zero (similarly to the bonding orbitals in diatomic molecules).

The π band with weakly overlapping $2p$ orbitals of atoms in a chain (which interact through the van der Waals mechanism) is characterized by the electron density periodicity described by the distance a_z between atoms along the z -axis, i.e. the band bottom corresponds to the momentum

$q_{0z} = \pi/a_z$. The probability $|F_\pi(q_{0z})|^2$ of finding such a momentum is large and close to the maximum of this function. In the basal (x, y) plane, we have $q_z = 0$ and for this reason the π band is not seen in Fig. 14.

Within the framework of the general discussion related to carbon properties, note that although the $(e, 2e)$ experiments have not been performed on diamond crystals, almost equivalent data are available for a silicon polycrystal having a structure of the same type [43]. The tetrahedral symmetry of diamond is characterized by sp^3 -hybridization, to which the σ band corresponds. The distinct feature of such a symmetry is the absence of the π band, which is observed in the experiment [43] shown in Fig. 15a. At the same time, because of the difference in the bonds C–C, Si–Si, and Si–C, an SiC crystal has sphalerite symmetry, which admits, along with the σ band, the π band as well. This band was observed in the $(e, 2e)$ experiment on an SiC polycrystal [3] (Fig. 15b). By the way, Fig. 15b illustrates in considerable degree what has been said in the preceding paragraph.

The tapping of the $(e, 2e)$ technique in the examples considered above did not result in the discovery of hitherto unknown properties of many-electron systems in a solid. However, this experimentation directly yielded, along with the PES technique, the dispersion curves of different types in the valence band of single crystals and thus successfully demonstrated its applicability in solid-state physics. The $(e, 2e)$ technique allows one to obtain similar dispersion curves for amorphous solids as well, where it gives completely new information which cannot be obtained by the PES.

The efficiency of the PES technique in studies of single crystals is based on the fact that the large component of the momentum q_z (see Section 1) can be compensated to a great extent by the displacement of all momenta by one of the momenta \mathbf{B} of a reciprocal lattice. This allows one to study, for example, the law of dispersion in the region of small quasi-momenta $\mathbf{q}' = \mathbf{q} - \mathbf{B}$. In the case of amorphous and other disordered structures, the PES technique can also be used for studying the dependence of the density of states on the energy ε but its efficiency is impaired in investigations of MDs, because in this case the Brillouin zone can no longer be displaced by the known momentum \mathbf{B} of the reciprocal lattice [121].

The $(e, 2e)$ study on the electron structure of amorphous carbon demonstrates the fundamental problems of the theory

of amorphous solids, posed by the experiment [39]. Another example related to amorphous germanium [24] will be briefly considered below.

Figure 16 shows electron MDs for the σ band of a graphite polycrystal and amorphous carbon (aC) for different electron binding energies ε [39]. In aC, the long-range order is absent but the short-range order is retained. The MD maxima which represent the δ -like peaks in a single crystal (for a given electron binding energy ε) are considerably smeared in the presence of short-range order only, but as one can see from Fig. 16 do not disappear. This degree of broadening reflects the order–disorder relation in a pithy manner (competition between the graphite-like and diamond-like structures, etc. [43]), but so far it has not been used to characterize the latter. It is remarkable that the electron MD in the valence band of aC is almost independent of the binding energy ε over a broad range from 8 to 20 eV.

A no less dramatic demonstration of the ‘cognitive ability’ of the $(e, 2e)$ technique is linked to the above-mentioned possibility of obtaining the MD directly for Bloch functions which are used in the tight-binding approximation [119] (see also Section 2.3). For this purpose, the summation of MDs for different electron binding energies should be performed, i.e. the spectral density should be integrated over the electron energy ε in the corresponding Brillouin zone. This was done, using the $(e, 2e)$ experimental results [121], in Ref. [120] for an ionic Al_2O_3 polycrystal with a rather complex structure. Each of the two aluminium atoms in the molecular cell of Al_2O_3 loses three electrons from the outer $3s^2$ and $3p^1$ orbitals and becomes an Al^{3+} cation. In contrast to that, each of the three oxygen atoms acquires two electrons and becomes an O^{2-} anion. This occurs in such a way that both the Al^{3+} cation and O^{2-} anion have the same electron configuration $1s^2 2s^2 2p^6$, i.e. a closed shell of neon. As a result, the outer orbitals in the Al_2O_3 molecular cell are mainly occupied by the $2s$ and $2p$ electrons of the oxygen atom, because the nuclear charge of the aluminium atom is much greater and therefore its $2s$ and $2p$ orbitals are bounded much stronger than in the oxygen atom.

Thus in the upper valence band of the aluminium oxide polycrystal, the $2p$ orbitals of the oxygen atom dominate, which are characterized by the specific MD whose maximum falls on the tangibly nonzero momentum (see above about atoms in a graphite single crystal). In the lower valence band,

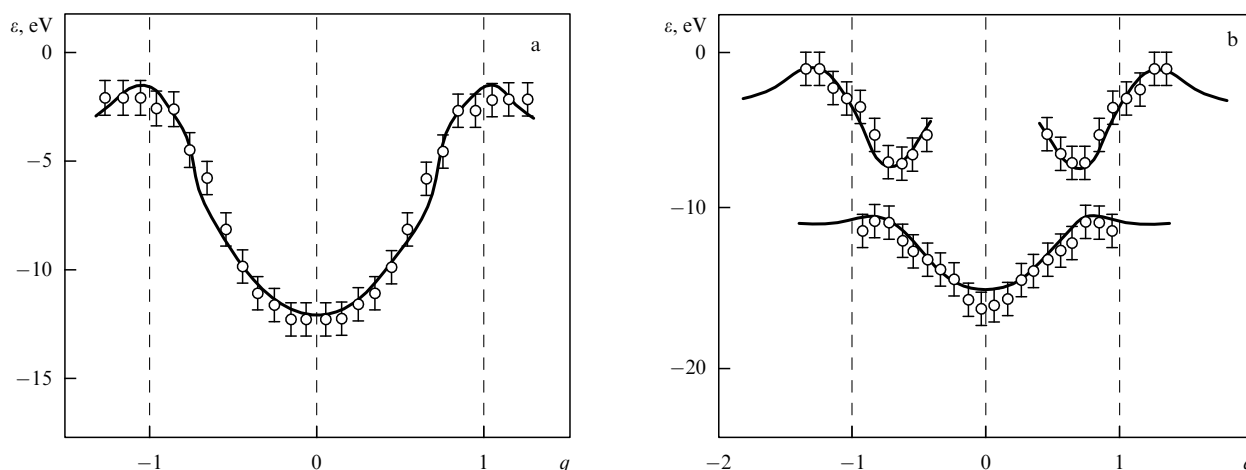


Figure 15. MDs of the maximum intensity, reflecting the law of dispersion $\varepsilon(\mathbf{q})$ for (a) amorphous silicon, and (b) silicon carbide [120].

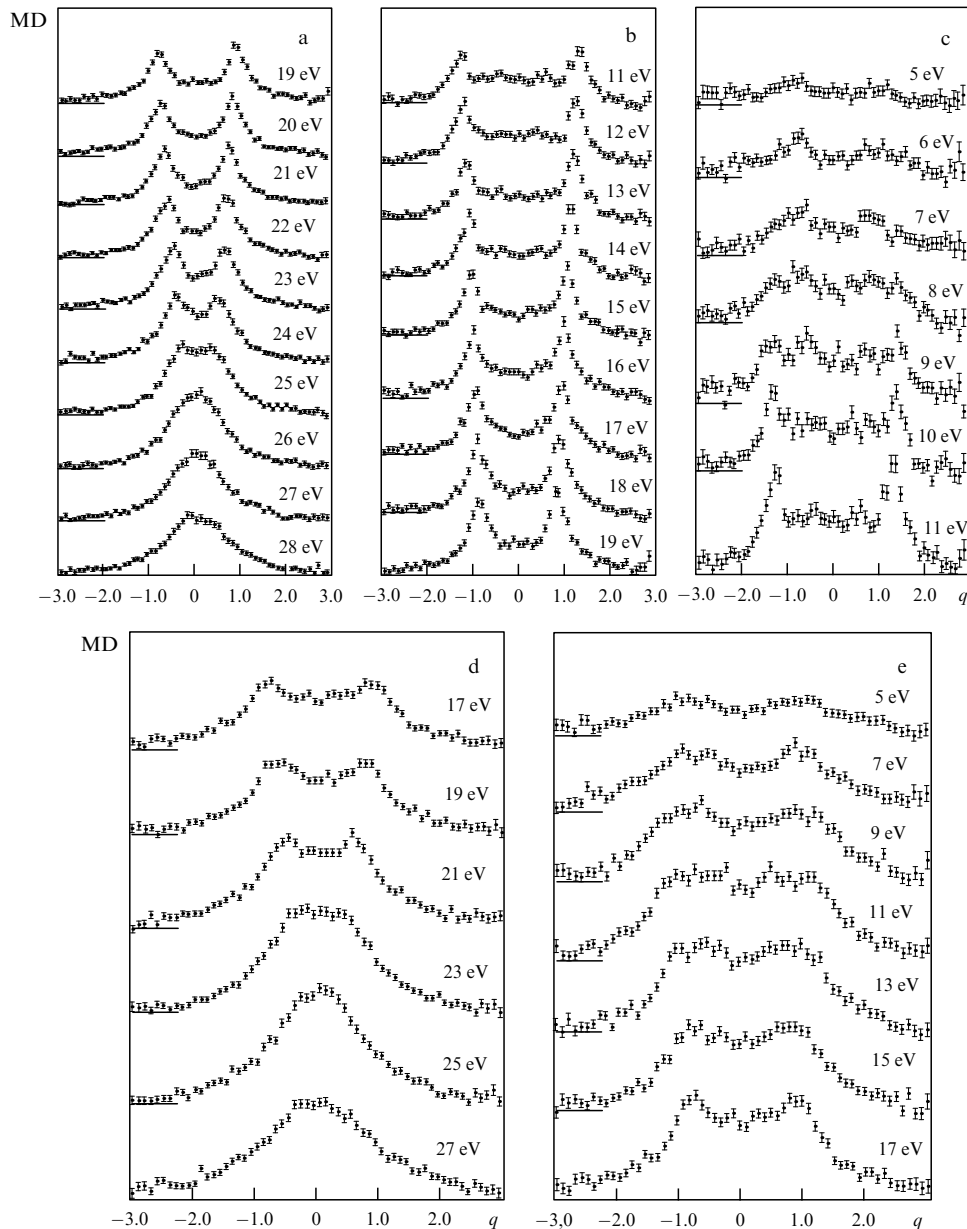


Figure 16. MDs for different electron binding energies within the valence band for (a–c) graphite polycrystal, and (d, e) amorphous carbon [39].

however, the $2s$ orbitals of oxygen are dominant, for which the MD maximum is located at zero. Actually, of course, one should bear in mind not simply dominating $2s$ and $2p$ oxygen orbitals but their linear combinations with the $3s$ and $3p$ orbitals of the aluminium atom. We shall call them for brevity the $2s$ and $2p$ type orbitals. The dispersion curve in the upper band is similar to that for the π band of a graphite crystal, and in the lower band — to that for the σ band of graphite [121]. Figure 17 shows MDs for the $2s$ and $2p$ type orbitals characterizing the valence bands of an Al_2O_3 polycrystal and firstly obtained in Ref. [120] by the above method. In particular, the $2p$ type orbital contains a small admixture of the s component, which suggests the presence of a so salient feature as a deviation from a pure ionic crystal structure. One may hope that similar measurements will soon be performed for other complex polycrystals.

Finally, as another example of the interesting possibilities of the (e,2e) technique, note the comprehensive study of

hydrogen adsorption by amorphous germanium (aGe) [43], where (as in the papers discussed above) the multiple scattering of electrons was considered. Comparison of the spectral densities $\rho(q, \varepsilon)$ of the aGe valence bands and hydrogen-adsorbing germanium (H–aGe) firstly showed that there are both regions where the value of $\rho(q, \varepsilon)$ is higher in aGe and where the value of $\rho(q, \varepsilon)$ is higher in H–aGe. Such nuances can be helpful in understanding the effect of adsorbed hydrogen on surface defects [43].

In conclusion of this section, we will formulate some accessible experimental problems which reflect our experience and seem interesting to us.

(1) The conduction band of transition metals is characterized by the hybridization from the orbitals of almost free s electrons and localized d electrons. For this reason, for instance, the electron MD pattern in a copper single crystal [24] should differ from that presented above for a simplest example of the conduction band of aluminium, demonstrat-

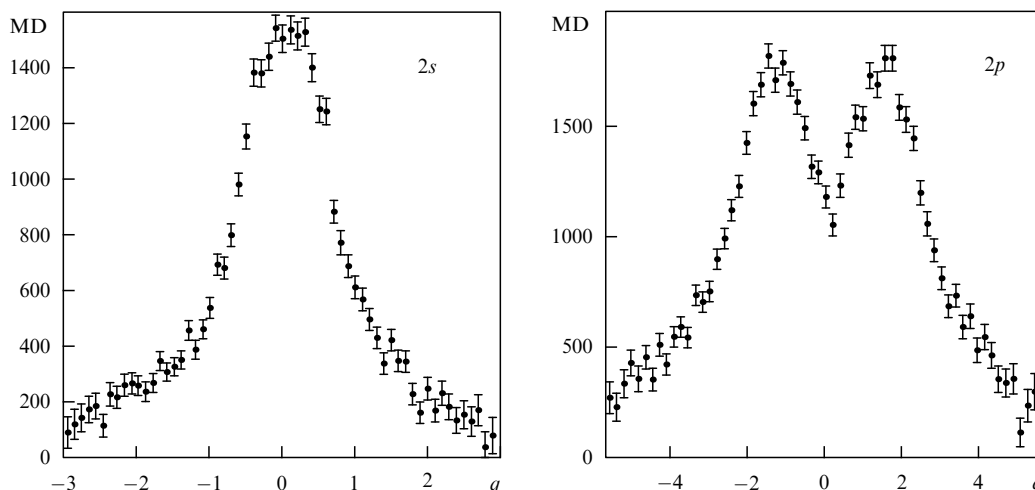


Figure 17. MDs for the $2s$ and $2p$ orbitals of an Al_2O_3 polycrystal [120].

ing properties of a Fermi gas. Specifically, the A_1 symmetry corresponds to the s electrons (the one-dimensional representation of a small group of the quasi-momentum \mathbf{k}), and the hybridization should be directly manifested in the shape of the electron MD along the $[111]$ direction in bands $\Gamma_1 A_1 L_1$ and $\Gamma'_{25} A_1 L'_2$ [27] (Fig. 18). To the left of the point of intersection of the curves (at $k/k_L \simeq 0.7$), the MD for the $\Gamma_1 A_1 L_1$ band has the dominating s component, while to the right — the d component. The opposite picture should be observed for the $\Gamma'_{25} A_1 L'_2$ band: the MD curve for the d electrons should tend to zero as k^4 for small k , whereas for the s electrons it should tend to a constant as for the Fermi gas. The $\Gamma_1 A_1 X_1$ and $\Gamma_{12} A_1 X'_4$ bands should reveal similar interrelated features along the $[100]$ direction.

The hybridization is absent for the bands corresponding to the two-dimensional representations of the above-mentioned group (to the A_3 representation). There are two such ‘purely d -electron’ bands (the s orbitals do not make contributions because they remain invariant upon the symmetry-group transformations of the crystal, viz. they correspond to the one-dimensional symmetric representation). However, for example, along the $[111]$ axis the electron MDs in these bands vanish, and other lower-symmetry directions should be used for their study [24].

Single crystals of transition metals represent a rich field open for $(e, 2e)$ experimental studies. The energy and

momentum resolutions achieved in this field are quite sufficient.

Of course, it is expedient to perform EMS studies in conjunction with PES [3]. The matter is that an electron with an energy of about 50 eV, emitted in the (γ, e) reaction, strongly interacts with the surface layer of the sample from which it is emitted. Bearing in mind the advantage of the high-energy resolution of PES, it is interesting to study the effect of the surface layer on the MDs of different shapes in single crystals of graphite, silicon, transition metals, etc., obtained both by the EMS and PES techniques.

The study of the valence electron orbitals in oxides of transition metals (see the above example of Al_2O_3) is also promising. This study can be used as a first step in the $(e, 2e)$ analysis of the electron structure of materials exhibiting the high-temperature superconductivity, in which the Cu–O bond plays an important role.

(2) We have mentioned above the problem of studying a plasmaron satellite in the conduction band of metals, whose existence was only suggested so far by the $(e, 2e)$ experiments [38, 44]. The achieved energy resolution $\Delta E \simeq 0.5 - 1.0$ eV is sufficient for this purpose [19], but the energy of each of the ejected electrons should exceed 10–15 keV in order to avoid intense multiple scattering accompanying the knock-out of strongly bounded electrons.

Unfortunately, the PES method has been employed so far for studying the interaction of electrons in solids with other collective excitations of the crystal lattice, phonons, resulting in the broadening (splitting) of the hole levels [3], because such a study requires the higher energy resolution ($\Delta E \sim 10^{-2}$ eV). Here, superconductivity physics is naturally the focus of attention [122].

(3) We formulated above the problem of the collective response of the conduction electrons in a metal to the ‘sudden’ appearance of a deep hole upon the electron knock-out from the atomic inner shell. The requirements on the values of ΔE and final energies E_1 and E_2 are obviously somewhat more stringent than for plasmaron study. In this connection, the unit with electron beam energy $E_0 = 50$ keV and symmetric kinematics, which is now in the making in Australia [19], promises especial urgency.

(4) We noted in Sections 3 and 4 that the Coulomb ee-correlations in atoms and molecules can be reliably

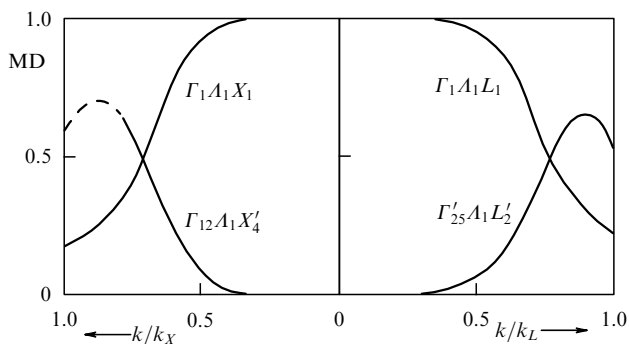


Figure 18. MDs for a copper single crystal: (a) along the $[100]$ direction, and (b) along the $[111]$ direction. Indices X and L denote boundaries of the Brillouin zone [27].

detected in the (e, 2e) reaction as a measurable transition to the satellite states of the ion with the excited electron configurations. In a solid, an analog of this could be, for example, the final satellite state with two holes in the conduction band and one excited electron in the higher-lying unfilled band. Such experiments have not been performed so far.

6. (e, 3e) ionization and electron–electron correlation spectroscopy

6.1 Choice of kinematics

In Section 3, we considered some successful approaches to the study of the ee-correlations by means of the (e, 2e) and (e, 2e)⁺ reactions both in many-electron systems, where they are realized via mixing of the HF configurations, and for a small number of electrons, where the correlators can be included in the trial wave functions in the explicit form (the Hilleraas functions). A natural continuation of this chain of reactions to a better understanding of the target structure is the double ionization of the target by an electron impact or the (e, 3e) process, when the energies and directions of momenta of all three knocked-on electrons are measured, and the so-called (e, 3–1e) reaction, when the direction of propagation of one of the electrons is not detected but its energy is measured.

The first theoretical papers on (e, 3e) ionization were reported by our group about 20 years ago [26, 49]. The first (e, 3e) and (e, 3–1e) experiments performed by the group of A Lahmam-Bennani in France [52, 123] and the group of M Coplan in USA [124] suggested the possibility of direct ee-correlation. This raised the question: What type of experimental kinematics are suitable for these purposes?

The (e, 3e) ‘coincidence’ experiments consist in the measurement of directions and energies of all emitted electrons involved in the reaction. The momenta of two from the three knocked-on electrons, for example \mathbf{p}_2 and \mathbf{p}_3 , can lie both in a plane formed by the vectors \mathbf{p}_0 and \mathbf{p}_1 and outside it, and their values can markedly vary within the limits of the laws of conservation. This provides rather great opportunities for theoretical studies and predictions. The theory of such processes even in the simplest case of a helium-atom target reduces to a theory of scattering of three charged particles in a central Coulomb field of a nucleus. This is a very complicated mathematical problem (see works [95, 96] and references cited therein), which virtually cannot be solved in the general form using computational methods.

One of the simplifying factors is the case when the energy of an incident electron is great compared to the transition energy (say, 5–10 keV in the event of the helium atom). If the energy of one of the knocked-on electrons, for example e_1 , is comparable to the energy of an incident electron, then such experimental kinematics (called dipolar kinematics in the modern scientific literature) allows one to describe fast electrons with plane waves. This approximation is realized at small transferred momenta Q , so that the dipolar (e, 3e) process is close (in physics of the collision mechanisms) to the double photoeffect.

In the experiments of Lahmam-Bennani’s group, reliable counting of triple coincidences was achieved for low energies E_2 and E_3 of the ejected electrons (10–25 eV). Such energies are obviously inadequate for reliable theoretical studies of a target by the double ionization technique, because the electron wave function of the final state $|\psi_f^-(\mathbf{p}_2, \mathbf{p}_3)\rangle$ is very

complex for calculations and estimates even for the helium atom.

Most of the simplifications in the scattering theory are achieved by increasing the energy of scattered particles. Then bearing in mind purely theoretical reasons, it seems desirable to enlarge the energy transferred to the electrons on retention of a small transferred momentum, so that both ejected electrons would have sufficiently large energies (say, 100–200 eV) and the electron wave function $|\psi_f^-(\mathbf{p}_2, \mathbf{p}_3)\rangle$ could be represented as a product of the plane, Coulomb or distorted waves, resulting in a considerable simplification of calculations. However, this assumption as a whole does not allow one to perform the correlation investigations exactly in a target.

Indeed, the nonsymmetrized wave function of the two ‘free’ interacting electrons in a field of the residual He⁺⁺ ion can be written in the general form as

$$\psi^-(\mathbf{p}_2, \mathbf{p}_3; \mathbf{r}_2, \mathbf{r}_3) = D(\mathbf{p}_2, \mathbf{p}_3) \times [\varphi^-(\mathbf{p}_2, \mathbf{r}_2), \varphi^-(\mathbf{p}_3, \mathbf{r}_3) + I(\mathbf{p}_2, \mathbf{p}_3; \mathbf{r}_2, \mathbf{r}_3)]. \quad (6.1)$$

The coefficient $D(\mathbf{p}_2, \mathbf{p}_3)$ appears due to the long-range Coulomb interactions and its modulus is equivalent to the Gamow factor

$$|D(\mathbf{p}_2, \mathbf{p}_3)|^2 = \frac{\pi x}{\exp(\pi x) - 1}, \quad x = p_{23}^{-1}$$

(the details can be brought up, for example, in Ref. [125]). For large energies E_2 and E_3 , the function $|D(\mathbf{p}_2, \mathbf{p}_3)|$ equals unity everywhere except the region of small angles θ_{23} , which we do not consider here. The function $I(\mathbf{p}_2, \mathbf{p}_3; \mathbf{r}_2, \mathbf{r}_3)$ also describes the multiple scattering of the ejected electrons in the final state. In turn, the one-particle function $\varphi^-(\mathbf{p}, \mathbf{r})$ at large energies can be written in the eikonal approximation as the product of the fast oscillating and smooth functions

$$\varphi^-(\mathbf{p}, \mathbf{r}) = \exp(i\mathbf{p}\mathbf{r}) \zeta(\mathbf{p}, \mathbf{r}). \quad (6.2)$$

As was mentioned above in Section 2.1, the distinctive property of (e, 2e) spectroscopy is a comparatively small recoil momentum q . The form factor (2.4) remains prominent exactly for small momenta q . In the case of the dipolar kinematics of the experiment, one has $q = |\mathbf{Q} - \mathbf{p}_2 - \mathbf{p}_3|$. The first term in square brackets in (6.1) describes the final state in the absence of the interaction between electrons 2 and 3, and large momenta p_2 and p_3 cannot appear in this case due to absorption of a real or virtual photon with the small momentum Q . This means that the contribution of the first term in sum (6.1) to the matrix element of the (e, 3e) process should be extremely small, although just this term is directly related to the double Fourier transform of the target wave function. A more detailed study showed that the characteristic structure in the scattering cross section, related to the first term in (6.1), is concentrated around the direction of the momentum \mathbf{Q} and has the asymptotic order of magnitude in the transferred energy $(\Delta E)^{-7}$ [126].

The second term in sum (6.1) can ‘mix’ momenta \mathbf{p}_2 and \mathbf{p}_3 due to the interaction of electrons, resulting in the regime $\mathbf{Q} \simeq \mathbf{p}_2 + \mathbf{p}_3$ or $q \simeq 0$. The structure in the scattering cross section related to the second term is concentrated around the direction of the momentum \mathbf{q} , and the characteristic peaks have the asymptotic order of magnitude $(\Delta E)^{-3}$ [126]. It is these peaks that we will ‘see’ first of all in the MD of the dipolar (e, 3e) process whose total cross section is extremely

small even so. The calculations performed in Ref. [126] confirm these simple qualitative considerations.

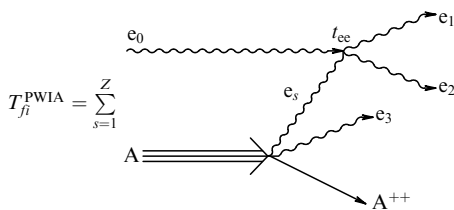
The function $I(\mathbf{p}_2, \mathbf{p}_3; \mathbf{r}_2, \mathbf{r}_3)$ in sum (6.1) governs the interaction of electrons in the final state, i.e. it distorts the direct information on the quasi-elastic impact phenomenon contained in the first term. This circumstance means that if some model of the target wave function yields the theoretical result coinciding with the experiment (say, in the approximation of a product of the orthogonalized Coulomb waves), then the function ψ_f^- accounting for the interaction of electrons after a collision event can completely destroy this coincidence, and the conclusion about the wave structure of a target will be incorrect.

Thus, from the above discussion follows that the kinematics of the (e, 3e) experiment even with comparatively large energies E_2 and E_3 of electrons ejected by a target under the action of a virtual photon with a small transferred momentum cannot be used for the direct spectroscopic investigations of electron correlations in atoms, although these kinematics are very attractive to experimentalists because of the large magnitudes of the corresponding cross sections.

6.2 Large transferred momenta. General formalism

The considerations presented in Section 6.1 suggest the choice of kinematics that retains the advantages of direct measurement of the Fourier transform of the target wave function without going to the region of the (e, 3e) measurement background. This is the kinematics in which a large energy of the incident electron is divided approximately equally between two of the three ejected electrons, i.e. we are dealing with the geometry of the quasi-elastic impact with a large transferred momentum.

The material of this section is mainly presented in papers [126, 127], and the concept was formulated in Ref. [49]. For the binary (e, 2e) reactions, the following conditions are typical: a plane geometry, $E_1 \simeq E_2 \simeq E_0/2$, and $\theta_1 \simeq \theta_2 \simeq 45^\circ$. The validity of these conditions for the binary (e, 3e) processes results in the PWIA approximation. The reaction can be illustrated by the following diagram



Recall that (E_0, \mathbf{p}_0) , (E_1, \mathbf{p}_1) , (E_2, \mathbf{p}_2) , and (E_3, \mathbf{p}_3) are the energies and momenta of the incident, scattered, as well as one and another ejected electrons, respectively, which satisfy the laws of conservation

$$E_{\text{tot}} = E_0 + \varepsilon_i = E_1 + E_2 + E_3 + \varepsilon_f, \quad (6.3)$$

$$\mathbf{p}_0 = \mathbf{p}_1 + \mathbf{p}_2 + \mathbf{p}_3 + \mathbf{q}. \quad (6.4)$$

Using the PWIA, we can write, similarly to Eqn (2.3), the expression for T_{fi}^{PWIA} in the analytic form

$$T_{fi} = Z^{1/2} F_{fi}(\mathbf{k}, \mathbf{p}_3) \langle \mathbf{p}_1, \mathbf{p}_2 | \hat{t}_{0z} (E_{\text{tot}} - \varepsilon_f - E_3) | \mathbf{p}_0, \mathbf{k} \rangle. \quad (6.5)$$

Here, the form factor $F_{fi}(\mathbf{k}, \mathbf{p}_3)$ equals the overlap integral

$$F_{fi}(\mathbf{k}, \mathbf{p}_3) = \int \exp(i\mathbf{k}\mathbf{r}_z) \psi_i(\mathbf{r}_1, \dots, \mathbf{r}_z) \times \psi_f^*(\mathbf{p}_3; \mathbf{r}_1, \dots, \mathbf{r}_{z-1}) \mathbf{d}\mathbf{r}_1 \dots \mathbf{d}\mathbf{r}_z, \quad (6.6)$$

and the notation $\mathbf{k} = \mathbf{Q} - \mathbf{p}_2 = \mathbf{p}_3 + \mathbf{q}$ was used for brevity.

The sixfold differential cross section for electron scattering can be written, similarly to Eqn (2.5), as

$$\frac{d^6\sigma}{d\Omega_1 d\Omega_2 d\Omega_3 dE_1 dE_2 dE_3} = \frac{Z p_1 p_2}{(2\pi)^5 p_0} \left(\frac{d\sigma}{d\Omega} \right)_{ee}^{\text{Mott}} \times \rho(\mathbf{p}_3, \mathbf{k}) \delta(E_1 + E_2 + E_3 + \varepsilon_{fi} - E_0), \quad (6.7)$$

where

$$\rho(\mathbf{p}_3, \mathbf{k}) = \frac{p_3}{(2\pi)^3} |F_{fi}(\mathbf{k}, \mathbf{p}_3)|^2. \quad (6.8)$$

The momenta \mathbf{p}_3 and \mathbf{k} in the last formula are assumed small, which allows one to make an asymptotic estimate of the cross section (6.7) as $(\Delta E)^{-3/2}$, which is the smallest of all the previous estimates.

Of course, the analysis of scattering cross section (6.7) cannot give a conclusion on the unambiguity of the determination of the initial-state wave function, however, we can try to find the stable specific features of the cross sections depending on the model type. To simplify the following analysis, we will restrict ourselves to the helium atom. This allows us, in turn, to simplify somewhat expression (6.7) by using partial expansions of the functions involved. After integration of Eqn (6.7) over dE_1 , we obtain the following expression for the fivefold differential cross section (5DCS):

$$\frac{d^5\sigma}{d\Omega_1 d\Omega_2 d\Omega_3 dE_2 dE_3} = \frac{2^5 p_1 p_2}{\pi^3 p_0} \left(\frac{d\sigma}{d\Omega} \right)_{ee}^{\text{Mott}} \times (1 - \exp(-4\pi/p_3))^{-1} \left| \sum_{l=0}^{\infty} (2l+1) \exp(i\sigma_l) P_l(\cos \theta_{\mathbf{k}\mathbf{p}_3}) \times \int_0^{\infty} r_1^2 j_l(kr_1) dr_1 \int_0^{\infty} r_2^2 R_l(p_3, r_2) \Phi_{0l}(r_1, r_2) dr_2 \right|^2, \quad (6.9)$$

where

$$R_l(p_3, r) = \left(\prod_{\mu=1}^l \sqrt{\mu^2 + \eta^2} \right) \times \frac{(2p_3 r)^l}{(2l+1)!} \exp(-ip_3 r) {}_1F_1[l+1 - i\eta, 2l+2; 2ip_3 r]$$

is the partial Coulomb function in the continuum. The cross section (6.9) can be further integrated over $d\Omega_3$, yielding the fourfold differential cross section (4DCS) for the (e, 3-1e) process in which the angles of a slow electron are not measured:

$$\frac{d^4\sigma}{d\Omega_1 d\Omega_2 dE_2 dE_3} = \frac{2^7 p_1 p_2}{\pi^2 p_0} \left(\frac{d\sigma}{d\Omega} \right)_{ee}^{\text{Mott}} \times (1 - \exp(-4\pi/p_3))^{-1} \sum_{l=0}^{\infty} (2l+1) \times \left| \int_0^{\infty} r_1^2 j_l(kr_1) dr_1 \int_0^{\infty} r_2^2 R_l(p_3, r_2) \Phi_{0l}(r_1, r_2) dr_2 \right|^2. \quad (6.10)$$

Comparison of expressions (6.9) and (6.10) shows that the $d^4\sigma$ cross section is a sum of squares of moduli of the partial amplitudes, whereas the $d^5\sigma$ cross section includes a direct

sum of the partial amplitudes, which takes into account the relative phases of the components. This suggests that analysis of the $d^5\sigma$ cross section can give much more information on the object under study. Notice also that the low energies E_3 of the ejected electrons do not lead, as in the case of nuclear forces, to the automatic disappearance of contributions from the nonzero harmonics, because the $R_l(p_3, r)$ function tends for $E_3 \rightarrow 0$ to a certain finite limit for any l , which reflects the parabolic rather than spherical symmetry of the final-state wave function.

Finally, expressions (6.9) and (6.10) can be easily generalized to the case of heavier atoms. To do this, the Coulomb phase σ_l should be replaced by $\sigma_l + \delta_l$, where the additional phase corresponds to electron scattering by a short-range potential of the mean intraatomic field, and the partial wave of scattering by the total potential should be considered for the function R_l .

6.3 (e, 3e) spectroscopy of electron correlations

Using the notation introduced in the previous section and assuming that the quasi-elastic (e, 2e) subprocess takes place, the momentum $-\mathbf{k}$ corresponds to the virtual momentum \mathbf{k}_1 of the electron knocked out from a pair. The another electron in the pair has the momentum $\mathbf{k}_2 = \mathbf{p}_3$. The momentum of the relative motion of the electrons in the pair and their center-of-mass momentum are equal to $\mathbf{k}_{12} = 1/2(\mathbf{k}_1 - \mathbf{k}_2)$ and $\mathbf{K} = \mathbf{k}_1 + \mathbf{k}_2$, respectively. A correlated electron pair (correlator) is formed when the average distance between the electrons is less than the average distance a_0 between the electrons in a target, i.e. $k_{12} > a_0^{-1}$. Because $K \simeq a_0^{-1}$, the momentum $k_{12} > K$, which represents the condition of the existence of the so-called quasi-free pair. In our notation, this condition has the form

$$\left| \mathbf{p}_3 + \frac{\mathbf{q}}{2} \right| > q$$

and is obviously satisfied for $q \simeq 0$. It follows from this inequality and expression (6.6) that for very small q the third-electron angular distribution is virtually uncorrelated with the direction of \mathbf{q} and is not coupled in energy with the quantity $q^2/2$ ('shaking off', according to Migdal [109]). As q increases, both the angular correlation and the energy coupling appear. This means that the experiment can really give the form of the ee-correlator in the many-electron wave function of the atomic target. The greater the momentum p_3 , the broader the range of variation of the recoil momentum q .

Indeed, if the momentum p_3 is sufficiently large for a plane wave to be separated in the function ψ_f , then formula (6.6) can be rewritten in the form

$$F_{fi}(\mathbf{k}, \mathbf{p}_3) = (Z - 1)^{1/2} \times \int e^{i\mathbf{q}\mathbf{r}_z + i\mathbf{p}_3(\mathbf{r}_z - \mathbf{r}_{z-1})} \psi_i(\mathbf{r}_1, \dots, \mathbf{r}_z) \psi_f^*(\mathbf{r}_1, \dots, \mathbf{r}_{z-2}) d\mathbf{r}_1 \dots d\mathbf{r}_z.$$

One can see that it is the dependence of the form factor on \mathbf{p}_3 that 'portrays' the rigid ee-correlator in the target. However, in this case the density ρ in Eqn (6.8) is extremely small compared to the momentum density of the quasi-elastic (e, 2e) scattering not only because of the presence of the factor $(2\pi)^{-3}$ equal approximately to 0.004, but also because the form factor itself is small and proportional to E_3^{-2} . For the density to be more or less noticeable, the values of q and p_3 should be comparatively small (no more than 2–2.5 au). Then it is highly conjectural to separate a plane wave from the

final-state wave function, and one should solve the multi-dimensional Schrödinger equation, when one slow electron finds itself in a continuum. This problem is very complex, except the case of the helium atom. It is for this reason that we considered here only this atom.

Comparison of Eqns (6.9) and (6.10) with Eqn (3.5) shows that the TDCS in formula (3.5) includes the overlap integrals between the target wave function and the discrete states of the Coulomb spectrum, whereas the 4DCS and 5DCS include analogous integrals containing Coulomb functions in the continuum. This circumstance suggests that additional information on the target can be obtained even for small momenta p_3 . To obtain qualitative estimates of the possibilities of (e, 3e) spectroscopy in this case, we chose three different simple functions which reproduced the electron binding energy in helium no worse than to 95%. These functions are described by expressions (3.10)–(3.12).

Figure 19 displays the $d^5\sigma$ cross sections for the binary process of the helium double ionization, which reflect the projection of the atomic wave function onto the continuous part of the Coulomb spectrum [128]. The fundamental difference of cross sections $d^5\sigma$ from $d^3\sigma$ [see Eqn (3.5)] is their additional dependence on the angle and energy of a slow

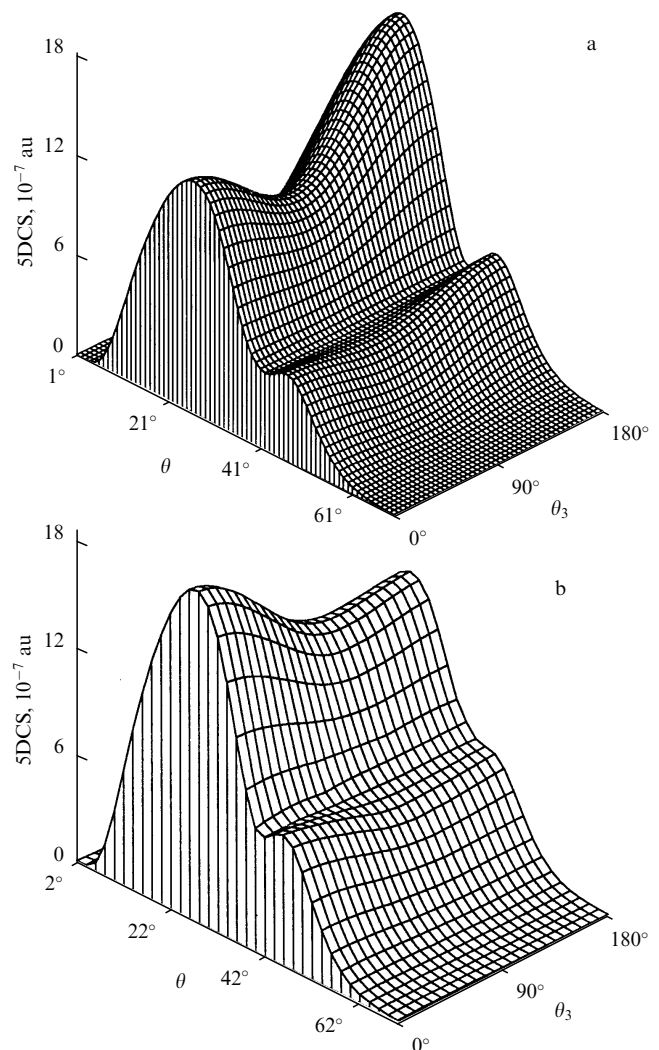


Figure 19. 5DCS as a function of the scattering angle θ and the angle θ_3 of a slow ejected electron for the $\text{He}(e, 3e)\text{He}^{++}$ reaction: (a) SPM (3.11); (b) H (3.12); $E_1 = E_2 = 250$ eV.

ejected electron e_3 . The shape of the cross section along the θ_3 axis even visually shows the contribution of the angular electron correlations. Thus, the angular correlations can be studied in a pure form by examining the dependence of the $d^5\sigma$ cross section on θ_3 .

Of interest, in our opinion, are also cross sections for the $(e, 3-1e)$ processes shown in Fig. 20 [128], from which it follows that in the case of models with radial correlations, a quasi-elastic peak splits into two peaks of different intensities, which does not occur for the typical HF function. In this case, different models accounting for the angular correlations do not change the characteristic feature as a whole, but affect the absolute values of cross sections. The partial term with $l = 0$ makes the main contribution to $d^4\sigma$ in the case of the SPM and H models. This result was expected because the contribution of the $(1s1s')$ state dominates in functions (3.11) and (3.12), while the role of the angular terms is small.

The dependence of the cross section (6.9) on the angles θ_1 and θ_2 of fast ejected electrons gives certain information on the presence and intensity of radial electron correlations in a target. The splitting of the quasi-elastic peak has here the same nature as in the case of $(e, 2e)^*$ reactions, which was discussed in detail in Section 3.2 (see Fig. 4). It is interesting to note that the shapes of TDCSs and 4DCSs are already very close for $n = 3$.

In conclusion of this section notice that a combination of $(e, 2e)$, $(e, 2e)^*$, and $(e, 3e)$ experimental data permits the formulation of the problem of complete diagnostics of the target wave function in the restricted region of angles and energies.

6.4 Comparative analysis of $(e, 3e)$ and $(\gamma, 2e)$ techniques for studying electron correlations

In this section we do not intend to describe in detail the rapidly developing field of multiple photoionization processes (which could be the subject of a separate review) but will perform only a comparative analysis of $(e, 3e)$ and $(\gamma, 2e)$ reactions for the electron correlation studies in a target over the region of high initial electron energies of interest to us. We

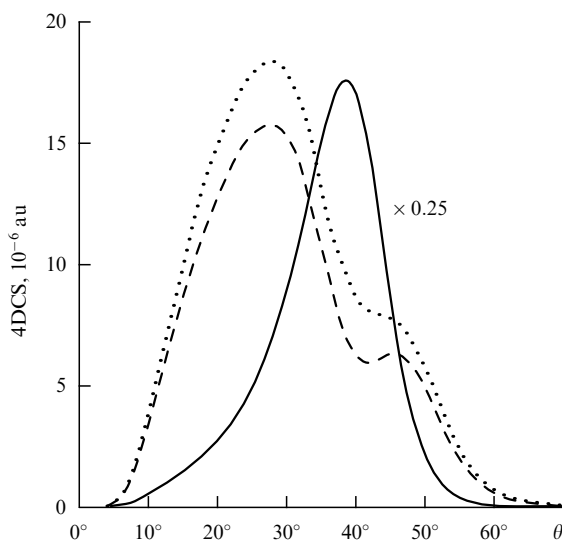


Figure 20. 4DCS as a function of the scattering angle θ for the $\text{He}(e, 3e)\text{He}^{++}$ reaction: the solid curve is the RHF function (3.10); the dashed curve is the SPM function (3.11); the dotted curve is the H function (3.12); $E_1 = E_2 = 250$ eV (cf. Fig. 3c).

showed in Sections 6.1–6.3 that in the case of the $(e, 3e)$ reaction, the most informative is the same kinematics of quasi-elastic knock-out, when the energy of the initial electron is about evenly divided between the scattered electron and one of the knocked-out electrons, whereas the second, slow electron leaves the target due to the rearrangement of the intraatomic field. In this case, the cross section is of the order of $10^{-6} - 10^{-7}$ au.

It was noted in paper [129] where the $(\gamma, 2e)$ processes were studied for atoms that the energy distribution curve for ejected electrons has a characteristic U shape with a broad minimum in the region of approximately equal energies, i.e. for $x = E_1/(E_1 + E_2) \approx 0.5$. This suggests that absorption of a photon by one of the atomic electrons dominates, whereas the second, slow electron is emitted due to the rearrangement of the self-consistent atomic field, caused by the ‘instant’ appearance of a hole [130]. This mechanism completely corresponds to the quasi-elastic knock-out in the $(e, 3e)$ reaction, however, in the case of the $(\gamma, 2e)$ ionization, the cross sections for such processes are extremely small. Let us show this by the example of the He atom. For more convenient comparison with the results of previous sections, we denote the fast and slow ejected electrons by the subscripts 2 and 3, respectively.

The fourfold differential cross section for the $(\gamma, 2e)$ process in the ‘velocity’ representation has the form (the speed of light in the atomic units is $c = \alpha^{-1} = 137$)

$$\begin{aligned} \frac{d^4\sigma}{d\Omega_2 d\Omega_3 dE_2 dE_3} &= \frac{\alpha p_2 p_3}{(2\pi)^4 E_\gamma} \\ &\times \delta(E_2 + E_3 + \epsilon_0^{\text{He}} - E_\gamma) \left| \iint d\mathbf{r}_1 d\mathbf{r}_2 \psi_i(\mathbf{r}_1, \mathbf{r}_2) \right. \\ &\times \left. [\exp(i\mathbf{Q}\mathbf{r}_1)(\mathbf{e}\vec{\nabla}_1) + \exp(i\mathbf{Q}\mathbf{r}_2)(\mathbf{e}\vec{\nabla}_2)] \psi_f^*(\mathbf{p}_2, \mathbf{p}_3; \mathbf{r}_1, \mathbf{r}_2) \right|^2. \end{aligned} \quad (6.11)$$

Here, $E_\gamma = \alpha^{-1}Q$, \mathbf{e} is the photon polarization vector, and $(\mathbf{e}\mathbf{Q}) = 0$. If the γ -quantum energy is almost completely transferred to one electron, then taking into account the symmetry of the helium wave function we can write approximately

$$\psi_f^-(\mathbf{p}_2, \mathbf{p}_3; \mathbf{r}_1, \mathbf{r}_2) \approx \frac{1}{\sqrt{2}} [e^{i\mathbf{p}_2\mathbf{r}_1} \varphi^-(\mathbf{p}_3, \mathbf{r}_2) + (\mathbf{r}_1 \leftrightarrow \mathbf{r}_2)].$$

Thus, the matrix element $M(\mathbf{p}_2, \mathbf{p}_3; \mathbf{Q})$ is a sum of the matrix elements M_1 and M_2 , where

$$\begin{aligned} M_1(\mathbf{p}_2, \mathbf{p}_3; \mathbf{Q}) &= \sqrt{2}(\mathbf{e}\mathbf{p}_2) \int \exp\{-i(\mathbf{p}_2 - \mathbf{Q})\mathbf{r}_1\} d\mathbf{r}_1 \\ &\times \int \varphi^{*-}(\mathbf{p}_3, \mathbf{r}_2) \psi_i(\mathbf{r}_1, \mathbf{r}_2) d\mathbf{r}_2, \\ M_2(\mathbf{p}_2, \mathbf{p}_3; \mathbf{Q}) &= i\sqrt{2}(\mathbf{e}\mathbf{p}_2) \int \exp(i\mathbf{Q}\mathbf{r}_1)(\mathbf{e}\vec{\nabla}_1) \varphi^{*-}(\mathbf{p}_3, \mathbf{r}_1) d\mathbf{r}_1 \\ &\times \int \exp(-i\mathbf{p}_2\mathbf{r}_2) \psi_i(\mathbf{r}_1, \mathbf{r}_2) d\mathbf{r}_2. \end{aligned} \quad (6.12)$$

The exchange process governed by the matrix element M_2 is, as a rule, asymptotically much weaker than the direct process, which is evident, by the way, from the form of the integrals, so that it can be neglected at large energies E_γ and E_2 . The direct

process could be not weak, if the quantity $\mathbf{k} = \mathbf{Q} - \mathbf{p}_2$ is small, as in the case of the (e, 3e) processes [cf. Eqn (6.8)]. However, due to the laws of dispersion $p_2 = \sqrt{2E_2}$, $Q = \alpha E_\gamma$, and if $E_\gamma \sim E_2$, then $p_2 \sim \sqrt{2/\alpha Q} \gg Q$. Typical energies E_γ of the synchrotron radiation are of the order of 10 keV, i.e. the photon momentum Q is approximately $3a_0^{-1}$, whereas the momentum p_2 is greater by a factor of ten. Thus, in contrast to (e, 3e) scattering, the value of k is large. Estimates of the cross section (6.11) with the matrix element M_1 yield the asymptotic order $E_\gamma^{-7/2}$, which is much smaller than the cross section of the (e, 3e) process [recall that in this case the cross section is proportional to $(\Delta E)^{-3/2}$].

Against this background, the probability of absorption of a photon by a virtual ee-pair with a large relative momentum becomes negligibly small. Even for energies $E_\gamma \simeq 500$ eV, the cross section for the double photoeffect with equal electron energies $E_2 = E_3$ is of the order of $10^{-6} - 10^{-8}$ au [131]. In addition, under such experimental kinematic conditions, the considerations presented in Section 6.1 become valid, where the ‘negative’ role of the ee-interaction in the final state was noted, which does not allow one to come to an unambiguous conclusion concerning the structural features of the target. This fact has also been pointed out in paper [51].

By this means binary (e, 3e) reactions permit studies in the region of energies and momenta inaccessible for double photoionization.

7. Conclusions

Thus, this review gives an insight into a kind of information on the structure of many-electron systems that can be obtained from studies of electron collisions at high energies, which are based on the conceptual experience of nuclear physics. The reviewed material well illustrates the known idea that the progress combining concepts and methods from different fields of science can yield original results having new physical meaning. One can see by the example of atoms that the EMS technique gives a detailed picture of mixing of the HF configurations. This method allows one to directly obtain, by exciting the satellite states, the MDs (and the corresponding probabilities) of electrons for the individual configurations appearing in the ground state of the many-electron system due to the effect of short-range ee-correlations. Moreover, the EMS of the excited states yields information on the ground-state wave function in the case of sufficiently strong radial correlations.

Studies of complex molecules have resulted in a nontrivial conclusion that the MDs of the outer-orbital electrons are very sensitive to the type of molecular conformation.

In the case of amorphous solids, EMS has no rivals in studies of both the band structure, dispersion curves, and MDs of electrons for different binding energies. This allows one to directly see the manifestation of the short-range order in the system.

The study of collective properties of the degenerate electron gas in metals by the (e, 2e) technique is a promising field in the physics of solids as well. Here, certain experimental progress is expected in the near future.

Finally, there are interesting possibilities for studying short-range ee-correlations in many-electron systems by their manifestation in binary (e, 3e) collisions.

As for the alternative prospects which have not been realized so far, they concern, for example, the quasi-elastic knock-out of atoms from molecules by atoms (in particular,

by helium atoms), accompanied by the production of free radicals as ‘final observing particles’ in the kinematically complete microscopic experiment. Within the framework of the EMS itself, the next significant step will be the use of polarized electron beams and polarization measurements, which is important for studying the role of the spin–orbit interaction in many-electron systems.

To conclude, the authors thank E Weigold, L V Vilkov, E A Vinogradov, V I Gol’danskii, A S Davydov, M Coplan, I McCarthy, E G Maksimov, V A Molchanov, V D Pis’mennyi, A T Rakhimov, N D Sokolov, N F Stepanov, G Stefani, S V Tyablikov, and N P Yudin for discussions and advice during different periods of these long studies. The authors also acknowledge C Brion for placing at our disposal some materials on the EMS of molecules, which we used in our review, G N Ogurtsov for valuable critical remarks, and K A Kuzakov and L I Gladneva for help in the preparation of the manuscript for publication.

This work was supported by the Interindustry Scientific and Technical Program ‘Physics of Quantum and Wave Processes’ of the Ministry of Science and Technical Politics of the Russian Federation.

References

- Vilkov L V, Pentin Yu A *Fizicheskie Metody Issledovaniya v Khimii: Strukturnye Metody i Opticheskaya Spektroskopiya* (Physical Methods of Studies in Chemistry: Structural Methods and Optical Spectroscopy) (Moscow: Vysshaya Shkola, 1987); *Stereochemical Applications of Gas Phase Electron Diffraction, Part A: Electron Diffraction Technique; Part B: Structural Information for Selected Classes of Compounds* (Eds I Hargitai, M Hargitai) (New York: VCH Publishers Inc., 1988)
- Dekhtyar I Ya *Phys. Rep.* **9** 243 (1974); Chuang S Y et al. *Phys. Lett. A* **88** 479 (1982); Singh A K et al. *Helv. Phys. Acta* **58** 640 (1985)
- Himpsel E J *Adv. Phys.* **32** 1 (1983); Hufner S *Photoelectron Spectroscopy: Principles and Applications* (Berlin: Springer-Verlag, 1995)
- Kheifets A S *Zh. Eksp. Teor. Fiz.* **89** 459 (1985) [*Sov. Phys. JETP* **62** 260 (1985)]
- Benning P J et al. *Phys. Rev. B* **44** 1962 (1991); Desjardins S J et al. *J. Chem. Phys.* **102** 6385 (1995)
- Smirnov Yu F, Neudatchin V G *Pis'ma Zh. Eksp. Teor. Fiz.* **3** 298 (1966) [*JETP Lett.* **3** 192 (1966)]
- Neudatchin V G, Novoskol'tseva G A, Smirnov Yu F *Zh. Eksp. Teor. Fiz.* **55** 1039 (1968) [*Sov. Phys. JETP* **28** 558 (1969)]
- Glassgold A E, Ialongo G *Phys. Rev.* **175** 151 (1968)
- Amaldi U, Jr. et al. *Rev. Sci. Instrum.* **40** 1001 (1969); Camilloni R et al. *Phys. Rev. Lett.* **29** 618 (1972)
- Weigold E, Hood S T, Teubner P J O *Phys. Rev. Lett.* **30** 475 (1973)
- Hood S T et al. *Phys. Rev. A* **8** 2494 (1973)
- Schneider J R et al. *Rev. Sci. Instrum.* **63** 1119 (1992)
- Hood S T, Hamnet A, Brion C E *Chem. Phys. Lett.* **39** 252 (1976)
- McCarthy I E, Weigold E *Phys. Rep. C* **27** 275 (1976)
- Stefani G, Camilloni R, Giardini-Guidoni A *Phys. Lett. A* **64** 364 (1978)
- Williams J F J *J. Phys. B* **11** 2015 (1978)
- Coplan M A et al. *J. Chem. Phys.* **71** 4005 (1979)
- Skillman T L et al. *Nucl. Instrum. Methods* **155** 267 (1978); Goruganthu R R et al. *J. Chem. Phys.* **89** 25 (1988)
- Storer P et al. *Rev. Sci. Instrum.* **65** 2214 (1994); Vos M et al. *Can. J. Phys.* **74** 829 (1996); Canney S et al. *J. Electron Spectrosc. Relat. Phenom.* **83** 65 (1997)
- Hayes P et al. *Rev. Sci. Instrum.* **59** 2445 (1988)
- Todd B R, Lermer N, Brion C E *Rev. Sci. Instrum.* **65** 349 (1994)
- Levin V G *Phys. Lett. A* **39** 125 (1972)
- Levin V G et al. *J. Chem. Phys.* **63** 1541 (1975); McCarthy I E *J. Phys. B* **8** 2133 (1975); Levin V G, Pavlichenkov A V *Phys. Lett. A* **58** 451 (1976)

24. Levin V G, Neudatchin V G, Smirnov Yu F *Phys. Status Solidi B* **49** 489 (1972)
25. Neudatchin V G, Zhivopistsev F A *Phys. Rev. Lett.* **32** 995 (1974); Zhivopistsev F A, Komarskiy F E *Fiz. Tverd. Tela* (Leningrad) **21** 924 (1979) [*Sov. Phys. Solid State* **21** 319 (1979)]
26. Neudatchin V G, Yudin N P, Zhivopistsev F A *Phys. Status Solidi B* **95** 39 (1979)
27. Vos M et al. *Phys. Rev. B* **51** 1866 (1995)
28. Kheifets A S, Cai Y Q, Vos M J. *Phys. C* **7** 1821, 3895 (1995)
29. Larkins F P, Richards J A J. *Phys. B* **14** 1477 (1981); *Chem. Phys.* **81** 329 (1983); Cook J P et al. *J. Phys. B* **17** 2339 (1984); Smith A D et al. *J. Phys. B* **19** 969 (1986)
30. Leung K T, Brion C E *Chem. Phys.* **82** 27 (1983)
31. McCarthy I E, Weigold E *Rep. Prog. Phys.* **54** 789 (1991)
32. Brion C E *Int. J. Quantum Chem.* **29** 1397 (1986); Brion C E, in *The Physics of Electronic and Atomic Collisions* (Eds T Andersen et al.) (New York: AIP Press, 1993) p. 350
33. Coplan M A, Moore J H, Doering J P *Rev. Mod. Phys.* **66** 985 (1994)
34. Davidson E R *Can. J. Phys.* **74** 757 (1996)
35. Duffy P *Can. J. Phys.* **74** 763 (1996)
36. Zheng Y, Neville J J, Brion C E *Science* **270** 786 (1995); Neville J J et al. *Can. J. Phys.* **74** 773 (1996)
37. Chao Gao et al. *Phys. Rev. B* **37** 3914 (1988)
38. Hayes P, Williams J F, Flexman J *Phys. Rev. B* **43** 1928 (1991)
39. Vos M et al. *Phys. Rev. B* **50** 5635 (1994)
40. Vos M et al. *Phys. Rev. B* **56** 963 (1997)
41. Cai Y Q et al. *Solid State Commun.* **95** 713 (1995)
42. Vos M et al. *Phys. Rev. B* **51** 3449 (1995)
43. Storer P et al. *J. Phys. D* **28** 2340 (1995); Vos M et al. *J. Phys. C* **7** 279 (1995); Cai Y Q et al. *Surf. Sci.* **334** 276 (1995)
44. Persiantseva N M, Krasil'nikova N A, Neudatchin V G *Zh. Eksp. Teor. Fiz.* **76** 1047 (1979) [*Sov. Phys. JETP* **49** 530 (1979)]
45. Dey S, Hayes P, Williams J F *J. Phys. D* **20** 504 (1987)
46. Van Wingerden B et al. *J. Phys. B* **14** 2475 (1981)
47. Stefani G, Camilloni R, Giardini-Guidoni A *J. Phys. B* **12** 2583 (1979)
48. Giardini-Guidoni A, Fantoni R, Tiribelli R *Phys. Lett. A* **77** 19 (1980)
49. Neudatchin V G et al. *Phys. Lett. A* **64** 31 (1977); Smirnov Yu F et al. *J. Phys. B* **11** 3587 (1978)
50. Levin V G et al. *J. Phys. B* **17** 1525 (1984)
51. Yudin N P, Pavlichenkov A V, Neudatchin V G *Z. Phys. A* **320** 565 (1985)
52. Lahmam-Bennani A, Dupre C, Duguet A *Phys. Rev. Lett.* **63** 1582 (1989)
53. Lahmam-Bennani A *J. Phys. B* **24** 2401 (1991)
54. Lahmam-Bennani A, Duguet A *Can. J. Phys.* **74** 837 (1996)
55. Lablanquie P et al. *Phys. Rev. Lett.* **58** 992 (1987); Price S D, Eland J H J. *Electron Spectrosc. Relat. Phenom.* **52** 649 (1990); Ouyama K, Eland J H, Kimura K *Phys. Rev. A* **41** 4930 (1990)
56. Von Raven E et al. *J. Electron Spectrosc. Relat. Phenom.* **52** 677 (1990)
57. Schwarzkopf O et al. *Phys. Rev. Lett.* **70** 2005 (1993); *J. Phys. B* **26** 1756 (1993)
58. Dörner R et al. *Phys. Rev. Lett.* **77** 4520 (1996)
59. Avaldi L et al. *J. Phys. IV (Coll. C6)(Paris)* **3** 145 (1993)
60. Volkov S S et al. *Yad. Fiz.* **52** 1339 (1990) [*Sov. J. Nucl. Phys.* **52** 848 (1990)]; Vorob'ev A A et al. *Yad. Fiz.* **58** 3 (1994) [*Phys. At. Nucl.* **58** 1 (1994)]
61. Den Herder J W A et al. *Nucl. Phys. A* **490** 507 (1988); Treland D G, Van Der Steenhoven G *Phys. Rev. C* **49** 2182 (1994); Bobeldijk I et al. *Phys. Lett. B* **353** 32 (1995)
62. Cowley A A et al. *Phys. Rev. C* **50** 2449 (1994)
63. Mougey G *Nucl. Phys. A* **335** 35 (1980); Frullani S, Mougey G, in *Adv. Nucl. Phys.* Vol 15 (Eds J V Negele, E Vogt) (New York: Plenum, 1983) p.1
64. Neudatchin V G, Yudin N P, Sviridova L L *Yad. Fiz.* **60** 2020 (1997) [*Phys. At. Nucl.* **60** 1848 (1997)]
65. Goldberger M L, Watson K M *Collision Theory* (New York: Wiley, 1964) [Translated into Russian (Moscow: Mir, 1967)]
66. Wu T-Y, Ohmura T *Quantum Theory of Scattering* (New York: Prentice-Hall Inc., 1962) [Translated into Russian (Moscow: Nauka, 1969)]
67. Neudatchin V G et al. *Phys. Rev. C* **50** 148 (1994); Tchuvilsky Yu M et al. *Phys. Rev. C* **51** 784 (1995); Neudatchin V G et al. *Yad. Fiz.* **58** 1234 (1995) [*Phys. At. Nucl.* **58** 1155 (1995)]
68. Sobel'man I I *Vvedenie v Teoriyu Atomnykh Spektrov* (Introduction to the Theory of Atomic Spectra) (Moscow: Nauka, 1977) [Translated into English as *Atomic Spectra and Radiative Transitions* (Berlin: Springer-Verlag 1979)]; Jucys A P, Savukinas A Yu *Matematicheskie Osnovy Teorii Atoma* (Mathematical Foundations of the Atomic Theory) (Vilnyus: Mintis, 1973)
69. Coulson C A, Duncanson W E *Proc. Camb. Phil. Soc.* **37** 406 (1941); **38** 100 (1942); **39** 10 (1943)
70. Moshinsky M *Harmonic Oscillator in Modern Physics* (New York: Gordon & Breach, 1969) [Translated into Russian (Moscow: Mir, 1972)]
71. Schrieffer J R *Theory of Superconductivity* (New York: W Benjamin Inc., 1964) [Translated into Russian (Moscow: Mir, 1968)]
72. Fritsch W, Lipperheide R, Wille U *Nucl. Phys. A* **198** 515 (1972); *Phys. Lett. B* **45** 103 (1973); Faessler A, Kusuno S, Strobel G L *Nucl. Phys. A* **203** 513 (1973)
73. Mahan G D *Phys. Rev.* **163** 612 (1967); Nozieres P, Dominicus S I *Phys. Rev.* **178** 1097 (1969); Nozieres P, Abrahams E *Phys. Rev. B* **10** 3099 (1974); Mahan G D *Many-Particle Physics* (New York: Plenum, 1991)
74. Langreth D C *Phys. Rev. B* **1** 471 (1970); Chang T T, Langreth D C *Phys. Rev. B* **5** 3512 (1972); Wertheim G K, Hüfner S *Phys. Rev. Lett.* **35** 53 (1975); Dow J D *Comments Solid State Phys.* **6** 71 (1975)
75. Lundqvist B I *Phys. Kondens. Materie* **6** 193, 206 (1967); **7** 117 (1968); **9** 231, 236 (1969); Aryasetiawan F, Hedin L, Karlsson K *Phys. Rev. Lett.* **77** 2268 (1996)
76. Weigold E *Nucl. Phys. A* **353** 327 (1981)
77. McCarthy I E *Can. J. Phys.* **74** 703 (1996); *Nucleus* **34** 181 (1997)
78. Giardini-Guidoni A et al., in *Electron and Photon Interactions with Atoms* (Eds H Kleinpoppen, M R C McDowell) (New York: Plenum Publ. Corp., 1976) p. 149; Camilloni R et al., in *Momentum Wave Functions-1976* (AIP Conf. Proc., Vol. 36) (New York: AIP Press, 1976) p. 205
79. Giardini-Guidoni A, Camilloni R, Stefani G, in *Coherence and Correlation in Atomic Collisions* (Eds H Kleinpoppen, J M Williams) (New York: Plenum Publ. Corp., 1979) p. 13
80. Clementi E, Roetti C *At. Data Nucl. Data Tables* **14** 177 (1974)
81. Avaldi L et al. *Phys. Rev. A* **33** 851 (1986); Popov Yu V et al. *Zh. Eksp. Teor. Fiz.* **90** 1191 (1986) [*Sov. Phys. JETP* **63** 694 (1986)]
82. Bonfert J, Graf H, Nakel W *J. Phys. B* **24** 1423 (1991)
83. Popov Yu V, Kuzmina N M *J. Phys. B* **26** 1215 (1993)
84. Walters H R J et al. *Z. Phys. D* **23** 353 (1992)
85. Van Wingerden B et al. *J. Phys. B* **12** L627 (1979)
86. Gélébart F, Tweed R J J. *Phys. B* **23** L621 (1990)
87. McCarthy I E et al. *Phys. Rev. Lett.* **33** 459 (1974); Dixon A J, McCarthy I E, Weigold E *J. Phys. B* **9** L195 (1976); Cook J P D et al. *J. Phys. B* **17** 2339 (1984)
88. Smith A D et al. *J. Phys. B* **19** 969 (1986)
89. Kuzakov K A, Popov Yu V *Vestn. Mosk. Gos. Univ. Ser. 3: Fiz. Astron.* **40** (2) 19 (1999)
90. Silverman J N, Platas O, Matsen F A J. *Chem. Phys.* **32** 1402 (1960)
91. Bonham R A, Kohl D A J. *Chem. Phys.* **45** 2471 (1966)
92. Temkin A *Phys. Rev.* **126** 130 (1962); Poet R J. *Phys. B* **11** 3081 (1978); **13** 2995 (1980); **14** 91 (1981); Ihra W et al. *Phys. Rev. A* **52** 3752 (1995)
93. Camilloni R et al. *Phys. Rev. A* **17** 1634 (1978)
94. Popov Yu V, Benayoun J J J. *Phys. B* **14** 3513 (1981)
95. Merkur'ev S P, Faddeev L D *Kvantovaya Teoriya Rasseyaniya dlya Sistem Neskol'kikh Chastits* (Quantum Scattering Theory of Few-Body Systems) (Moscow: Nauka, 1985) [Translated into English: Faddeev L D, Merkuriev S P *Quantum Scattering Theory for Several Particle Systems* (Dordrecht: Kluwer Acad. Publ., 1993)]
96. Shablov V L, Shitkov Yu Yu, Popov Yu V *Fundam. Prikl. Mat.* **2** 925 (1996); Shablov V L, Bilyk V A, Popov Yu V *Fundam. Prikl. Mat.* **4** 1207 (1998)
97. Gailitis M, in *(e, 2e) and Related Processes* (London: Kluwer Acad. Publ., 1992) p. 273
98. McCarthy I E, Weigold E *Phys. Rep.* **27** 275 (1976); Camilloni R et al. *J. Phys. B* **13** 397 (1980)

99. Maslov V P *Asimptoticheskie Metody v Teorii Vozmushchenii* (Asymptotic Methods in the Perturbation Theory) (Moscow: Nauka, 1988)
100. Zheng Y et al. *Chem. Phys.* **188** 109 (1994)
101. Zheng Y et al., Preprint ESM-121 (Adelaide: Flinders Univ. of South Australia, 1996)
102. Bawagan A D O, Brion C E *Chem. Phys.* **123** 51 (1988)
103. Rolke J, Brion C E *Chem. Phys.* **207** 173 (1996)
104. Clark S A C, Bawagan A D O, Brion C E *Chem. Phys.* **137** 407 (1989)
105. Bawagan A D O et al. *Chem. Phys.* **113** 19 (1987)
106. Labanowski J, Andzelm J (Eds) *Density Functional Methods in Chemistry* (New York: Springer-Verlag, 1991)
107. Kohn W, Sham L *Phys. Rev. A* **190** 1123 (1965)
108. Frost L et al. *Chem. Phys.* **113** 1 (1987); Frost L et al. *Chem. Phys.* **119** 253 (1988); Grisogino A M et al. *Chem. Phys.* **124** 121 (1988)
109. Migdal A B, Kraĭnov V P *Priblizhennyye Metody Kvantovoi Mekhaniki* (Approximation Methods in Quantum Mechanics) (Moscow: Nauka, 1966) [Translated into English (New York: W A Benjamin, 1969)]; Migdal A B *Kachestvennyye Metody v Kvantovoi Teorii* (Qualitative Methods in Quantum Theory) (Moscow: Nauka, 1975) [Translated into English (Redwood City, Calif.: Addison-Wesley Publ. Co., 1977)]; Dykhne A M, Yudin D L *Usp. Fiz. Nauk* **125** 377 (1978) [*Sov. Phys. Usp.* **21** 549 (1978)]
110. Hellebone B P et al. *Chem. Phys.* **173** 193 (1994)
111. Adcock W et al. *J. Am. Chem. Soc.* **119** 2896 (1997)
112. McMillan K et al. *J. Am. Chem. Soc.* **94** 8648 (1990)
113. Tossell J A, Moore J H, Coplan M A *Chem. Phys.* **67** 356 (1979)
114. Rolke J et al. *Chem. Phys.* **215** 191 (1996)
115. Engleman R *The Jahn–Teller Effect in Molecules and Crystals* (New York: Wiley, 1972)
116. Vos M, Bottema M *Phys. Rev. B* **54** 5946 (1996)
117. Canney S A et al. *J. Phys. C* **9** 1931 (1997)
118. Zhivopistsev F A, Comas F E *Phys. Status Solidi B* **100** 303 (1980); Zhivopistsev F A, Komasa F E *Fiz. Tverd. Tela* (Leningrad) **21** 924 (1979) [*Sov. Phys. Solid State* **21** 319 (1979)]
119. Ziman J M *The Calculation of Bloch Functions* (New York: Academic Press, 1971) [Translated into Russian (Moscow: Mir, 1973)]
120. Vos M, McCarthy I E *Rev. Mod. Phys.* **67** 713 (1995); Vos M, Preprint ESM-132 (Adelaide: Flinders Univ. of South Australia, 1996)
121. Guo X et al. *Phys. Rev. B* **54** 17943 (1996)
122. Ginzburg V L, Maksimov E G *Sverkhprovodimost': Fiz., Khim., Tekh.* **5** 1543 (1992) [*SPCT* **5** (9) 1505 (1992)]
123. Lahmam-Bennani A et al. *J. Phys. B* **24** 3645 (1991)
124. Ford M J et al. *Rev. Sci. Instrum.* **66** 3137 (1995); Ford M J et al. *Phys. Rev. A* **51** 418 (1995)
125. Popov Yu V *J. Phys. B* **14** 2449 (1981)
126. Popov Yu V et al. *J. Phys. B* **27** 1599 (1994); Popov Yu V et al. *Zh. Eksp. Teor. Fiz.* **107** 337 (1995) [*JETP* **80** 179 (1995)]; Popov Yu V, Dal Cappello C *Can. J. Phys.* **74** 843 (1996)
127. Popov Yu V, Dal Cappello C, Kuzakov K J. *Phys. B* **29** 5901 (1996)
128. Popov Yu V, Kuzakov K A *Vestn. Mosk. Gos. Univ. Ser. 3: Fiz. Astron.* **40** (2) 16 (1999)
129. Carlson T A *Phys. Rev.* **156** 142 (1967)
130. Brown R L *Phys. Rev. A* **1** 586 (1970)
131. McCarthy I E et al. *Phys. Rev. A* **40** 3041 (1989)